

WING FILE COPY

6

AD-A206 242



USE OF NAVIER-STOKES METHODS TO PREDICT
CIRCULATION CONTROL AIRFOIL PERFORMANCE

THESIS

Steven L. Williams

AFIT/GAE/AA/89M-4

S DTIC
ELECTE
APR 04 1989
DOS

DISTRIBUTION STATEMENT A
Approved for public release
Distribution Unlimited

DEPARTMENT OF THE AIR FORCE
AIR UNIVERSITY

AIR FORCE INSTITUTE OF TECHNOLOGY

Wright-Patterson Air Force Base, Ohio

89 4 03 038

1

AFIT/GAE/AA/89M-4

DTIC
S ELECTE
APR 04 1989
D *cb*

USE OF NAVIER-STOKES METHODS TO PREDICT
CIRCULATION CONTROL AIRFOIL PERFORMANCE

THESIS

Steven L. Williams

AFIT/GAE/AA/89M-4

Approved for public release; distribution unlimited

USE OF NAVIER-STOKES METHODS TO PREDICT
CIRCULATION CONTROL AIRFOIL PERFORMANCE

THESIS

Presented to the faculty of the School of Engineering
of the Air Force Institute of Technology
Air University
In Partial Fulfillment of the
Requirements for the Degree of
Master of Science in Aeronautical Engineering



Steven L. Williams, B.S.

March 1989

| | |
|--------------------|-------------------------------------|
| Accession For | |
| NTIS CRA&I | <input checked="" type="checkbox"/> |
| DTIC TAB | <input type="checkbox"/> |
| Unannounced | <input type="checkbox"/> |
| Justification | |
| By | |
| Distribution | |
| Availability Codes | |
| Dist | Avail and/or Special |
| A-1 | |

Approved for public release; distribution unlimited

List of Figures

| <u>Figure</u> | <u>Page</u> |
|---|-------------|
| 1. Circulation Control Airfoil | 2 |
| 2. Circulation Control Airfoil Computational O-Grid Boundaries | 15 |
| 3. Turbulence Model Curvature Correction Characteristics | 20 |
| 4. Interior Region of Airfoil Computational Grid | 24 |
| 5. Jet Slot and Coanda Surface Region of Airfoil Computational Grid | 25 |
| 6. Close-up of Slot Region of Airfoil Computational Grid | 26 |
| 7. 103RE Circulation Control Airfoil Geometry | 27 |
| 8. Correlation of Computational and Experimental Blowing Coefficients | 30 |
| 9. Variation of Computational and Experimental Lift Coefficient with Blowing Coefficient | 31 |
| 10. Variation of Computational and Experimental Pitching Moment Coefficient with Blowing Coefficient | 33 |
| 11. Variation of Computational and Experimental Drag Coefficient with Blowing Coefficient | 33 |
| 12. Computational and Experimental Pressure Coefficient Distributions (Point 33) | 35 |
| 13. Airfoil Region Computational Mach Contours, $C_{\mu} = 0$ (Point 33) | 37 |
| 14. Coanda Surface Region Computational Mach Contours, $C_{\mu} = 0$ (Point 33) | 37 |
| 15. Coanda Surface Region Computational Velocity Vectors, $C_{\mu} = 0$ (Point 33) | 38 |
| 16. Computational and Experimental Pressure Coefficient Distributions (Point 35) | 39 |
| 17. Airfoil Region Computational Mach Contours, $C_{\mu} = 0.0096$ (Point 35) | 41 |

Acknowledgements

It is only fitting that some time be taken to acknowledge the substantial support of those that have made this effort possible. I am deeply indebted to Dr Franke, my thesis advisor, for providing much needed guidance and support over the last few years as I struggled to get my degree on a part-time basis. I also wish to thank Dr Visbal of the Flight Dynamics Lab for the use of his Navier-Stokes code and making time in his busy schedule to answer my many questions. I wish to especially thank Jane Abramson of the David Taylor Naval Ship Research and Development Center for providing me with the experimental data used in this study and expert advice. I also wish to express my appreciation to George Shrewsbury of the Lockheed-Georgia Company for being a valuable resource and patiently answering my questions about turbulence modeling.

Most of all, I am thankful for the encouragement and support from my wife, Vicky, without whose love and unfailing support this effort would not have been possible. You are very special. Lastly, I wish to dedicate this work to my Lord and Savior, Jesus Christ, the foundation of my life and one who gives life true meaning.

Steven L. Williams

Table of Contents

| | <u>Page</u> |
|---|-------------|
| Acknowledgements | ii |
| List of Figures | iv |
| List of Tables | vi |
| List of Symbols | vii |
| Abstract | x |
| I. Introduction | 1 |
| Background | 4 |
| Objective | 7 |
| II. Approach | 9 |
| Governing Equations and Numerical Formulation | 9 |
| Boundary Conditions | 14 |
| Turbulence Model | 18 |
| Grid | 22 |
| Computer Resources | 24 |
| III. Results and Discussion | 27 |
| 103RE Airfoil | 27 |
| Force and Moment Comparison | 29 |
| Point 33 Results | 34 |
| Point 35 Results | 39 |
| Point 36 Results | 42 |
| Point 38 Results | 46 |
| Computed Jet Characteristics | 49 |
| Solution Sensitivity to Curvature Constant | 51 |
| Use of the Method in a Design Environment | 56 |
| IV. Conclusions | 60 |
| V. Recommendations | 62 |
| Appendix: 103RE Airfoil Coordinates | 63 |
| Bibliography | 68 |
| Vita | 70 |

| <u>Figure</u> | <u>Page</u> |
|---|-------------|
| 18. Coanda Surface Region Computational Mach Contours, $C_{\mu} = 0.0096$ (Point 35) | 41 |
| 19. Coanda Surface Region Computational Velocity Vectors, $C_{\mu} = 0.0096$ (Point 35) | 42 |
| 20. Computational and Experimental Pressure Coefficient Distributions (Point 36) | 43 |
| 21. Airfoil Region Computational Mach Contours, $C_{\mu} = 0.0187$ (Point 36) | 44 |
| 22. Coanda Surface Region Computational Mach Contours, $C_{\mu} = 0.0187$ (Point 36) | 45 |
| 23. Coanda Surface Region Computational Velocity Vectors, $C_{\mu} = 0.0187$ (Point 36) | 45 |
| 24. Computational and Experimental Pressure Coefficient Distributions (Point 38) | 47 |
| 25. Airfoil Region Computational Mach Contours, $C_{\mu} = 0.0332$ (Point 38) | 48 |
| 26. Coanda Surface Region Computational Mach Contours, $C_{\mu} = 0.0332$ (Point 38) | 48 |
| 27. Coanda Surface Region Computational Velocity Vectors, $C_{\mu} = 0.0332$ (Point 38) | 49 |
| 28. Variation of Computational Jet Slot Exit Velocity Profiles with Blowing Coefficient | 50 |
| 29. Variation of Computational Jet Detachment Point with Blowing Coefficient | 51 |
| 30. Variation of Computational Lift Coefficient with Curvature Constant (Point 38) | 52 |
| 31. Variation of Computational Pitching Moment Coefficient with Curvature Constant (Point 38) | 54 |
| 32. Variation of Computational Drag Coefficient with Curvature Constant (Point 38) | 54 |
| 33. Computational and Experimental Pressure Coefficient Distributions, $\theta = 3.2$ (Point 38) | 55 |

List of Tables

| <u>Table</u> | <u>Page</u> |
|--|-------------|
| 1. 103RE Airfoil Computational and Experimental Test Conditions | 28 |
| 2. Typical Navier-Stokes Run Times on Different Computers | 58 |

List of Symbols

| <u>Symbol</u> | <u>Definition</u> |
|---------------|---|
| c | Airfoil chord length |
| c_p | Specific heat at constant pressure |
| C_d | Section drag coefficient, Eq (22) |
| C_{d_f} | Section friction drag coefficient |
| C_{d_p} | Section pressure drag coefficient |
| C_l | Section lift coefficient |
| $C_{m_{.5}}$ | Section pitching moment coefficient about 50% chord |
| C_p | Pressure coefficient |
| C_v | Momentum blowing coefficient. Eq (21) |
| e | Internal energy per unit mass |
| F | Bradshaw curvature correction factor, Eq (24) |
| J | Jacobian |
| l | Turbulence model mixing length |
| \dot{m} | Jet mass flow rate |
| M | Local Mach number |
| M_∞ | Freestream Mach number |
| n | Local normal coordinate direction |
| p | Static pressure |
| p_t | Jet total pressure |
| p_∞ | Freestream static pressure |
| q_∞ | Freestream dynamic pressure |
| r | Local streamline radius of curvature |
| Pr | Prandtl number |
| Pr_t | Turbulent Prandtl number |
| R | Perfect gas constant |

| <u>Symbol</u> | <u>Definition</u> |
|--------------------|---|
| R_e | Reynolds number |
| s | Distance in n-coordinate direction |
| S | Turbulence model curvature term, Eq (25) |
| t | Time |
| T | Static temperature |
| T_t | Jet total temperature |
| U | Local velocity |
| U_∞ | Freestream velocity |
| V_j | Jet velocity |
| u, v | Velocity components in Cartesian coordinate axes |
| \bar{U}, \bar{V} | Contravariant velocity components, Eq (3) |
| x, y | Cartesian coordinate axes |
| α | Airfoil angle of attack |
| α_{eff} | Airfoil effective angle of attack |
| δ | Jet detachment angle |
| γ | Specific heat ratio |
| θ | Bradshaw empirical curvature constant |
| μ | Viscosity |
| μ_t | Turbulent eddy viscosity |
| ρ | Static density |
| ρ_∞ | Freestream static density |
| τ | Transformed time |
| ϕ | Slot angle relative to the x-coordinate direction |
| ω | Vorticity |
| ξ, η | Transformed coordinates |

Subscripts

Definition

| | |
|-------|---|
| inner | Inner layer of Baldwin-Lomax turbulence model |
| NS | Navier-Stokes |
| WT | Wind tunnel |

Abstract

The predictive capability of the two-dimensional compressible mass-averaged Navier-Stokes equations was investigated for a typical circulation control airfoil. The governing equations were solved using the implicit approximate-factorization algorithm of Beam-Warming with the turbulence model of Baldwin-Lomax. To account for the unique characteristics of circulation control airfoils, an empirical turbulence model correction due to Bradshaw was employed. This study is unique in that the predictive capability of the computational method is explored by examining the importance of the empirical Bradshaw curvature correction constant on the computed results.

Using a generic value of the curvature constant at various blowing coefficient levels, the computational method was able to accurately predict the airfoil pitching moment and lift curve slope due to blowing. Predicted levels of airfoil lift coefficient, although reasonable, were found to be consistently low compared with experiment due to the generic curvature constant providing premature jet detachment from the Coanda surface. Computed and measured airfoil drag results followed the same trends, but the lack of overall drag coefficient agreement was somewhat disappointing.

Lift coefficient was found to be quite sensitive, pitching moment not sensitive, and drag coefficient moderately sensitive to the value of curvature constant used. For the highest blowing coefficient case considered, the value of curvature constant required for the computational lift coefficient to match the experimental lift coefficient was also determined. Using the experimentally correlated curvature constant, very good agreement between the computational and experimental pressure distributions was found.

In spite of the sensitivity of the computational results to the Bradshaw curvature correction constant, the method provided relatively accurate predictions of airfoil performance for the circulation control airfoil used in this study. Based on this result, the computational method shows promise as a circulation control airfoil design tool.

USE OF NAVIER-STOKES METHODS TO PREDICT
CIRCULATION CONTROL AIRFOIL PERFORMANCE

I. Introduction

The development of short takeoff and landing (STOL) aircraft with conventional aircraft cruise performance has long been a goal of aircraft design engineers (8:6-8). Such a STOL aircraft would greatly reduce the need for large areas of land for conventional airports next to thriving metropolitan areas where land is in great demand. Due to decreased landing speeds and the capability for steeper climbout and approach paths, STOL aircraft offer increased flight safety and reduced noise pollution. The use of STOL military aircraft would lessen the dependence on undamaged runways for operational capability. Advantages such as these make STOL aircraft an attractive proposition.

Unfortunately, designing a STOL aircraft with conventional aircraft performance is not an easy task. To gain STOL performance, devices must be added to an aircraft which degrade its cruise performance either through external changes to the aircraft or additional weight. Many different concepts for STOL aircraft have been proposed over the years. One such promising concept is circulation control.

Circulation control makes use of the well known Coanda effect. The Coanda effect, simply stated, says that a stream of fluid introduced tangentially next to a curved convex surface will tend to remain attached, even through large turning angles (5:53,18:2). Circulation control airfoils utilize the Coanda effect by blowing a small, high-velocity jet over a rounded airfoil trailing edge. A typical circulation control airfoil is shown in Figure 1. Since the airfoil trailing edge is not

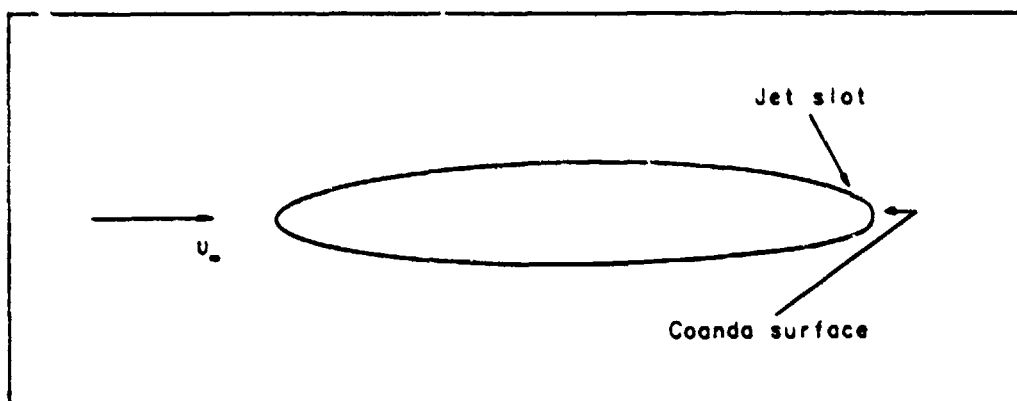


Figure 1. Circulation Control Airfoil

sharp, as on conventional airfoils, the Kutta condition is not fixed for a range of angle of attack, but set by the amount of airfoil blowing. The resulting movement of the front and rear stagnation points toward the lower airfoil surface results in increased circulation and, hence, increased lift.

Use of this unique concept offers certain advantages and disadvantages over conventional airfoils. Circulation control airfoils can attain lift coefficients much greater than conventional airfoils at low speeds due to the Coanda effect.

This capability allows an aircraft to takeoff and land at greatly reduced speeds and still attain the same value of lift. Circulation control airfoils generate lift by blowing engine bleed air over the Coanda surface rather than angle of attack as on conventional airfoils (18:2). Thus, the aircraft does not have to use pitch on takeoff and landing, resulting in greater pilot visibility. Another advantage of circulation control airfoils is that they do not use complex mechanical flaps (8:163). One of the disadvantages of circulation control airfoils is that due to their blunt, rounded trailing edge, they have poorer performance at cruise speeds when compared with conventional airfoils. The use of blowing also requires the addition of pressurized ducts to the aircraft which results in increased aircraft weight.

Some excellent references are available concerning the state of circulation control technology. One such paper by Wood and Nielsen (18) presents a complete review of the field along with some discussion of important parameters concerning circulation control airfoil performance. Another paper by Nielsen and Biggers (9) presents a summary of the Circulation-Control Workshop held at the NASA Ames Research Center in 1986. At this meeting a wide variety of papers were presented concerning circulation control airfoil theory and experiment.

Background

Determining the performance of circulation control airfoils using theoretical or computational methods has been proven to be extremely difficult due to the complex flowfield involved. The flow over a circulation control airfoil is greatly complicated by the rounded trailing edge, or Coanda surface, and the introduction of jet blowing. The jet boundary-layer detachment from the Coanda surface must be accurately found due to the great sensitivity of lift to the forward and aft stagnation point locations. The wall-jet flow from the slot also introduces a second boundary layer into the flowfield with different length scales than the conventional airfoil boundary layer. In addition, a free shear layer is formed between the oncoming airfoil upper surface boundary layer and the wall-jet flow. Also, as the jet blowing increases, so does the influence of compressibility, even at relatively low freestream Mach numbers.

Due to the highly coupled non-linear behavior of the flowfield, the Navier-Stokes equations appear to offer the best hope of solving this complicated problem. Solutions using coupled lesser approximations of the Navier-Stokes equations, such as TRACON (7), do not appear to offer the needed accuracy for circulation control airfoil design purposes (18:18). However, solutions of circulation control airfoil flowfields seriously challenge even Navier-Stokes methods due to the lack of accurate turbulence models for highly curved flows with strong adverse pressure gradients.

One of the first studies concerning the use of Navier-Stokes methods in evaluating circulation control airfoil performance was conducted by Berman (4). Berman solved for the flow over a circulation control airfoil using TRACON over the first 50% of the airfoil chord and a McCormack explicit solver with the Baldwin-Lomax turbulence model over the aft 50% chord. This method was able to obtain solutions showing correct trends with the experimental pressure coefficient distribution, however, the magnitudes of the computed pressure coefficients were not as large as those found experimentally. Berman states that "reliance on the inflow conditions from TRACON proved to be a major obstacle" (4:6) in the study. Evidently, the coupling between TRACON and the Navier-Stokes method proved too weak to properly model the resulting flowfield.

Shrewsbury (12-14) examined the use of an implicit formulation of the compressible Reynolds-averaged Navier-Stokes equations with a modified form of the Baldwin-Lomax turbulence model. Jet slot boundary conditions were set at the slot exit and a correction due to Bradshaw was applied to the turbulence model to account for the curvature of the Coanda surface. A variety of airfoils at different flight conditions were examined. This method performed well, obtaining lift and pressure coefficient results in close agreement with experimental data. Although good overall agreement was reached, Shrewsbury concluded that better turbulence models were needed to better resolve the jet detachment from the Coanda surface (13:6).

Pulliam et al. (10) also employed an implicit formulation of the Navier-Stokes equations with the Baldwin-Lomax turbulence model to compute the flow over circulation control airfoils. However, Pulliam applied a turbulence model correction suggested by Baldwin and, instead of using a conventional grid topology, used a spiral grid. The spiral grid extended from the jet plenum chamber through the slot exit and was wrapped about the airfoil. Use of this unique grid scheme allowed the flow to be computed rather than modeled at the jet slot exit. This study examined two different circulation control airfoils at varying flight conditions and obtained results in close agreement with experiment. However, since the results were not completely predictive, due to the need to adjust the turbulence model for different cases, Pulliam also concluded that better turbulence models were needed (10:146).

These papers have demonstrated that the Navier-Stokes equations can indeed provide good estimates of the lift and pitching moment of circulation control airfoils at various flight conditions provided the turbulence model is able to give a reasonably good estimate of the jet separation point from the Coanda surface. Unfortunately, the turbulence model curvature corrections used by both Shrewsbury and Pulliam contain an empirical constant term whose magnitude is dependent on the type of airfoil Coanda surface and the freestream Mach number of the flow (10:144). Thus, to obtain solutions of comparable accuracy, one must, through trial and error, determine the value of the empirical constant which yields a computational solution

in close agreement with the experimental data. To predict airfoil performance for design purposes, where little or no experimental data is available, this approach is unacceptable.

Objective

The purpose of this study is to explore the predictive capability of Navier-Stokes methods in determining the performance of circulation control airfoils. To accomplish this goal, a computational method very similar to the one used by Shrewsbury is developed and applied to a typical circulation control airfoil. The method used in this study solves the two-dimensional compressible mass-averaged Navier-Stokes equations using the implicit approximate-factorization algorithm of Beam-Warming. Closure of these equations for turbulent flows is obtained using the Baldwin-Lomax turbulence model with a curvature correction due to Bradshaw. However, rather than demonstrate that the Navier-Stokes equations can model circulation control airfoil flows, which has been done already, this study examines the importance of the empirical turbulence model correction in obtaining accurate predictions of airfoil performance. This is done by first applying the method with a generic, predefined value of the empirical curvature constant at various blowing coefficients and comparing the results with experiment. Then the sensitivity of the computational results to a range of curvature constant values is explored. In this manner, the actual capability of Navier-Stokes methods to predict the performance of circulation control airfoils can be

assessed. In addition, some discussion is also included concerning possible use of the method for circulation control airfoil design.

II. Approach

The main challenge in this study was to first obtain a Navier-Stokes capability to solve the circulation control airfoil problem. Initially, an attempt was made to obtain the computer program used by Shrewsbury in his investigations. Unfortunately, this program was considered company proprietary software and could not be obtained. Possible use of the method developed by Pulliam was also examined. However, since a conventional grid generator was already available in-house, this method was not considered because of its need for a specialized spiral grid. As a result, a proven, conventional airfoil Navier-Stokes solver developed by the Air Force was obtained and modified to solve for circulation control airfoil geometries. The modifications to the chosen method consisted of modifying the airfoil boundary conditions to account for jet slot blowing and employing the turbulence model curvature correction of Bradshaw to account for the curvature of the Coanda surface. Discussion of the resulting method, airfoil grid and computer resources used in this study are contained in the following sections.

Governing Equations and Numerical Formulation

The Navier-Stokes solver chosen for use in this study was developed by Dr M.R. Visbal of the Air Force Wright Aeronautical Laboratories. The formulation of this method, as well as its validation with experimental data, has been well documented in

the literature (15-17). This section briefly summarizes this method.

The governing equations are the two-dimensional compressible mass-averaged Navier-Stokes equations which consist of the continuity equation, the momentum equations, and the energy equation. These equations have been formulated using a general time-dependent curvilinear coordinate transformation:

$$\begin{aligned}\xi &= \xi(x, y, t) \\ \eta &= \eta(x, y, t) \\ \tau &= t\end{aligned}\tag{1}$$

The governing equations may be cast in the following strong-conservation form:

$$\partial_{\tau} q + \partial_{\xi} E_1 + \partial_{\eta} E_2 = \partial_{\xi} (V_1 + V_2) + \partial_{\eta} (W_1 + W_2)\tag{2}$$

where

$$q = J^{-1}(\rho, \rho u, \rho v, \rho e)$$

$$E_1 = \frac{1}{J} \begin{bmatrix} \rho \bar{u} \\ \rho u \bar{u} + \xi_x p \\ \rho v \bar{u} + \xi_y p \\ (p + \rho e) \bar{u} - \xi_t p \end{bmatrix}$$

$$E_2 = \frac{1}{J} \begin{bmatrix} \rho \bar{v} \\ \rho u \bar{v} + \eta_x p \\ \rho v \bar{v} + \eta_y p \\ (p + \rho e) \bar{v} - \eta_t p \end{bmatrix}$$

$$v_1 = \frac{1}{J} \begin{bmatrix} 0 \\ b_1 u_\xi + b_2 v_\xi \\ b_2 u_\xi + b_3 v_\xi \\ b_1 u u_\xi + b_2 (v u + u v_\xi) + b_3 v v_\xi + b_4 T_\xi \end{bmatrix}$$

$$v_2 = \frac{1}{J} \begin{bmatrix} 0 \\ c_1 u_\eta + c_2 v_\eta \\ c_3 u_\eta + c_4 v_\eta \\ c_1 u u_\eta + c_2 u v_\eta + c_3 v u_\eta + c_4 v v_\eta + c_5 T_\eta \end{bmatrix}$$

$$w_1 = \frac{1}{J} \begin{bmatrix} 0 \\ c_1 u_\xi + c_3 v_\xi \\ c_2 u_\xi + c_4 v_\xi \\ c_1 u u_\xi + c_2 v u_\xi + c_3 u v_\xi + c_4 v v_\xi + c_5 T_\xi \end{bmatrix}$$

$$w_2 = \frac{1}{J} \begin{bmatrix} 0 \\ d_1 u_\eta + d_2 v_\eta \\ d_2 u_\eta + d_3 v_\eta \\ d_1 u u_\eta + d_2 (v u_\eta + u v_\eta) + d_3 v v_\eta + d_4 T_\eta \end{bmatrix}$$

$$b_1 = (\nu + \nu_t) \left(\frac{4}{3} \xi_x^2 + \xi_y^2 \right)$$

$$b_2 = \frac{1}{3} (\nu + \nu_t) \xi_x \xi_y$$

$$b_3 = (\nu + \nu_t) \left(\xi_x^2 + \frac{4}{3} \xi_y^2 \right)$$

$$b_4 = c_p \left(\frac{\nu}{p_r} + \frac{\nu_t}{p_{r_t}} \right) (\xi_x^2 + \xi_y^2)$$

$$c_1 = -(\mu + \mu_t) \left(\frac{4}{3} \xi_x \eta_x + \xi_y \eta_y \right)$$

$$c_2 = -(\mu + \mu_t) \left(\frac{2}{3} \xi_x \eta_y - \xi_y \eta_x \right)$$

$$c_3 = (\mu + \mu_t) \left(\xi_x \eta_y - \frac{2}{3} \xi_y \eta_x \right)$$

$$c_4 = -(\mu + \mu_t) \left(\xi_x \eta_x + \frac{4}{3} \xi_y \eta_y \right)$$

$$c_5 = -c_p \left(\frac{\mu}{p_r} + \frac{\mu_t}{p_{r_t}} \right) (\xi_x \eta_x + \xi_y \eta_y)$$

$$d_1 = (\mu + \mu_t) \left(\frac{4}{3} \eta_x^2 + \eta_y^2 \right)$$

$$d_2 = \frac{1}{3} (\mu + \mu_t) \eta_x \eta_y$$

$$d_3 = (\mu + \mu_t) \left(\eta_x^2 + \frac{4}{3} \eta_y^2 \right)$$

$$d_4 = c_p \left(\frac{\mu}{p_r} + \frac{\mu_t}{p_{r_t}} \right) (\eta_x^2 + \eta_y^2)$$

The contravariant velocity components are denoted by

$$\bar{u} = \xi_t + \xi_x u + \xi_y v$$

$$\bar{v} = \eta_t + \eta_x u + \eta_y v$$

(3)

and

$$\xi_t = (-x_\tau y_\eta + y_\tau x_\eta)J$$

$$\xi_x = y_\eta J$$

$$\xi_y = -x_\eta J$$

$$\eta_t = (x_\tau y_\xi - y_\tau x_\xi)J \quad (4)$$

$$\eta_x = -y_\xi J$$

$$\eta_y = x_\xi J$$

$$J = \frac{1}{(x_\xi y_\eta - x_\eta y_\xi)}$$

are the transformation metrics.

Closure of this system of equations is provided by the perfect gas law, Sutherland's viscosity formula and the assumption of constant Prandtl number. To obtain turbulent solutions of the governing equations, a modified version of the Baldwin-Lomax turbulence model is used.

The governing equations are solved numerically using the implicit approximate-factorization scheme of Beam-Warming (3). In this formulation, first-order Euler time differencing is used while the spatial derivative terms are discretized using second-order accurate central differences. Both explicit and implicit smoothing terms have been added to the algorithm for numerical stability and to capture embedded shocks (15:19-21). A variable time step can be employed for faster convergence to a

steady-state solution. This solver is fully vectorized for use on parallel processing computers.

Boundary Conditions

In order to solve the set of equations describing the fluid motion, proper boundary conditions need to be defined. In the case of a circulation control airfoil, with the flow at the jet slot modeled, a blowing boundary condition must be set at the jet slot exit. All other boundary conditions are identical to those found for conventional airfoils. Shown in Figure 2, the set of required boundary conditions can be broken down into those required for the exterior grid boundary, grid cut line, airfoil surface and jet slot.

Along the inflow portion of the exterior grid, freestream conditions are used. These correspond to

$$u = U_{\infty} \cos \alpha \quad (5)$$

$$v = U_{\infty} \sin \alpha \quad (6)$$

$$p = p_{\infty} \quad (7)$$

$$\rho = \rho_{\infty} \quad (8)$$

Along the outflow portion of the exterior grid, a subsonic outflow is assumed. The outflow boundary conditions are

$$\frac{\partial u}{\partial x} = 0 \quad (9)$$

$$\frac{\partial v}{\partial x} = 0 \quad (10)$$

$$\frac{\partial p}{\partial x} = 0 \quad (11)$$

$$p = P_{\infty} \quad (12)$$

The derivative boundary conditions in Eqs (9), (10) and (11) are approximated using a first-order accurate extrapolation.

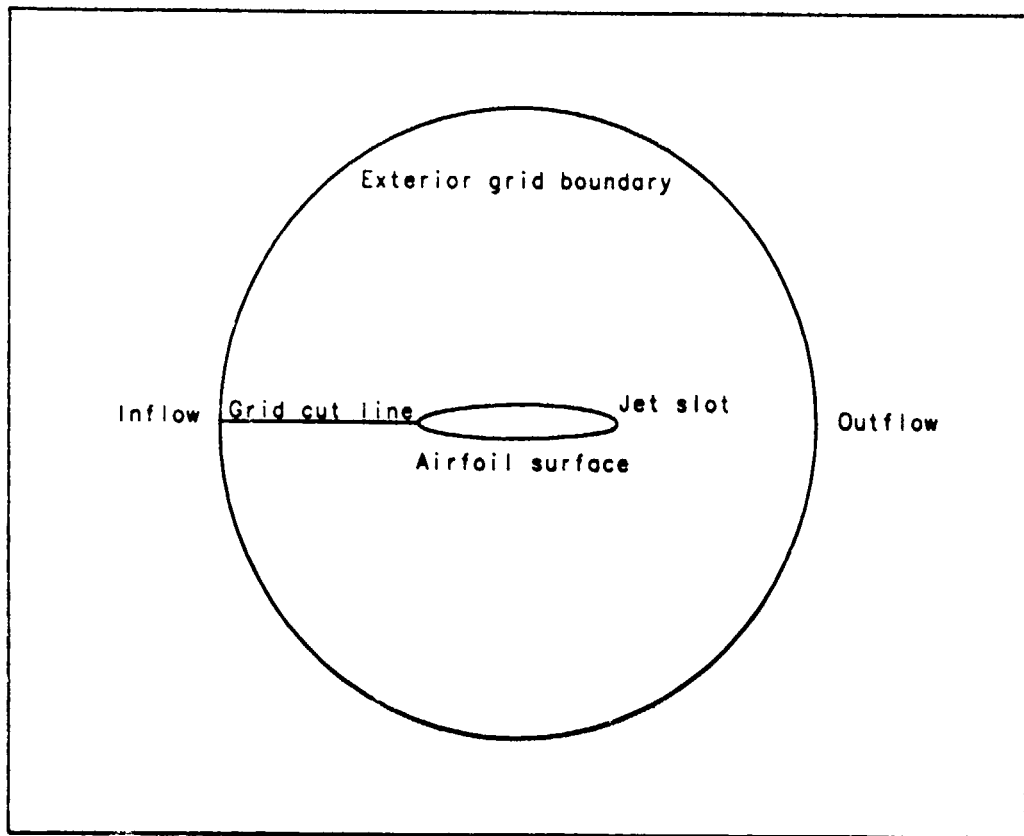


Figure 2. Circulation Control Airfoil Computational O-Grid Boundaries

Along the grid cut line a periodic boundary condition is enforced. This is accomplished by using a five-station grid point overlap in the wrap-around direction. In this overlap region, all flow variables are set equal at each grid point.

Everywhere on the airfoil surface, except the jet slot, the following adiabatic, no-slip boundary conditions are used:

$$u = 0 \quad (13)$$

$$v = 0 \quad (14)$$

$$\frac{\partial p}{\partial n} = 0 \quad (15)$$

$$\frac{\partial T}{\partial n} = 0 \quad (16)$$

The derivative boundary conditions in Eqs (15) and (16) are approximated using zero-order and second-order accurate extrapolations, respectively.

Certain assumptions, based upon the work of Shrewsbury (13:4), are made to set the boundary conditions at the jet slot exit. First, it is assumed that the jet total pressure and total temperature are constant across the slot exit. Second, it is assumed that the isentropic relations provide a good approximation of the internal flow before the slot exit. Third, The jet nozzle is assumed to be convergent. With these assumptions, the slot exit boundary conditions are

$$\frac{\partial p}{\partial x} = 0 \quad (17)$$

$$T = T_t \left(1 + \frac{\gamma-1}{2} M^2\right)^{-1} \quad (18)$$

$$u = M(\gamma RT)^{1/2} \cos\phi \quad (19)$$

$$v = M(\gamma RT)^{\frac{1}{2}} \sin \phi \quad (20)$$

From Eq (17), the static pressure at the slot exit is first determined using a second-order accurate extrapolation. Then, using the isentropic relation relating the ratio of static pressure to jet total pressure, the local Mach number at the slot exit can be determined. The other flow variables at the jet slot exit can then be found using Eqs (18), (19) and (20).

The boundary conditions at the jet slot exit are modified if the local flow exceeds a sonic velocity at the slot exit. This is due to the limiting condition of choked flow which will occur for a convergent nozzle with the throat area at the slot exit. If a local Mach number greater than one is computed using Eq (17) and the isentropic relation relating pressure ratio to Mach number, the local flow is set to Mach one to simulate a choked condition. The pressure, density and temperature are then set to their respective critical values for a choked condition at the given jet total pressure and total temperature.

Control of the jet momentum blowing coefficient for a given case is controlled by adjusting the jet total pressure ratio, jet total temperature ratio and jet slot height. These three quantities determine the boundary conditions at the slot exit and the resulting jet mass flow rate. The momentum blowing coefficient is found using

$$C_{\mu} = \frac{\dot{m}_j v_j}{q_{\infty} c} \quad (21)$$

In Eq (21), the jet velocity is determined assuming an

isentropic expansion of the jet total pressure to freestream static pressure.

The calculation of airfoil drag coefficient is also modified to account for the added effect of jet thrust using

$$C_d = C_{d_f} + C_{d_p} - C_\mu \quad (22)$$

found in reference (7). Using Eq (22), it is possible to obtain negative values of drag coefficient at high jet blowing rates.

Turbulence Model

In simulating any turbulent flow, accuracy of the turbulence model is of crucial importance. This is especially true of the solution about a circulation control airfoil. Determining the point of boundary-layer detachment from the Coanda surface is critical in obtaining accurate solutions. Unfortunately, the present state of knowledge concerning the turbulent modeling of highly curved flows with strong adverse pressure gradients is far from complete. However, a reasonable qualitative understanding of these flows has been formulated along with some empirical approximations in the literature.

The turbulence model used in this study is the algebraic model of Baldwin-Lomax (2). This turbulence model is the most widely used of all Navier-Stokes turbulence models due to its simplicity and accuracy for a wide range of turbulent flows. However, to accurately model the curved flow over the Coanda surface this turbulence model requires some modification.

It appears from experimental observation that the effects of curvature can have both a stabilizing as well as destabilizing influence on boundary-layer development (5:3). For circulation control airfoils a convex curvature is encountered by the boundary layer as it moves over the Coanda surface. The effect of convex curvature can have one of two effects on the boundary layer depending on the gradient of velocity in the direction normal to the airfoil surface. If velocity increases with increasing distance normal to the convex surface, the boundary layer will tend to become more stable. If the velocity decreases with increasing distance normal to the convex surface, the boundary layer will tend to become more turbulent in behavior.

To empirically correct the Baldwin-Lomax turbulence model to account for the effects of streamline curvature, a method suggested by Bradshaw (5:68-71) is used. In determining the turbulent eddy viscosity of the inner layer (2:2), the Baldwin-Lomax turbulence model uses the following equation:

$$(\nu_t)_{\text{inner}} = \rho \omega l^2 \quad (23)$$

Bradshaw empirically adjusts the magnitude of the mixing length in Eq (23) to account for streamline curvature by multiplying it by a curvature correction factor:

$$F = 1 - 6S \quad (24)$$

where

$$S = \frac{U}{r} \frac{\partial U}{\partial n} \quad (25)$$

In the Eqs (24) and (25), all the quantities necessary to determine the curvature correction factor can be found from the flowfield solution with the exception of θ which is the empirical curvature correction constant.

The behavior of the mixing length correction is in proper agreement with the experimentally observed trends as shown in Figure 3. Figure 3 denotes a typical boundary-layer profile just downstream of the slot exit on the Coanda surface. This

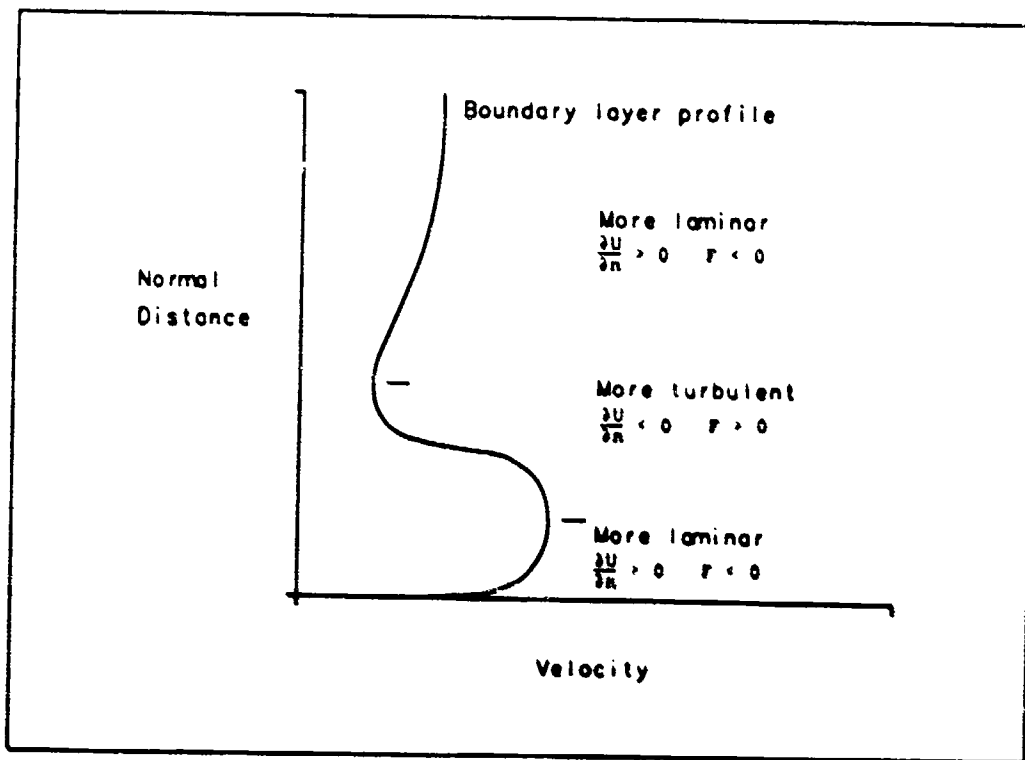


Figure 3. Turbulence Model Curvature Correction Characteristics

correction has a singularity whenever the velocity gradient is zero, which occurs whenever a velocity minimum or maximum occurs in the profile. As a result, an abrupt change in the character of the correction occurs at these points.

Bradshaw cautions that this model should only be used as a linear correction. From the limited experimental data available, he suggests that

$$0.5 < F < 1.5 \quad (26)$$

and

$$\theta = 6 \quad (27)$$

The use of Eq (26) essentially limits the influence of the curvature correction to the linear range and alleviates some of the difficulties encountered when the correction changes character. Eq (27) refers to the generic value of curvature correction constant suggested for unstable wall jets (5:70). In this study, the Bradshaw curvature correction is employed with the Baldwin-Lomax turbulence model using Eqs (26) and (27), unless otherwise noted.

The boundary-layer transition criteria used in this study is different than that proposed by Baldwin-Lomax (2:2) and based upon the investigation of transition found in Schlichting (11:489-505). The transition criteria used in this study includes the effects of Reynolds number and pressure gradient on transition location. The transition location downstream of the forward stagnation point on both upper and lower airfoil

surfaces is first determined by assuming that the point of boundary-layer instability is identical to the point of boundary-layer transition. This point can be found given the flight Reynolds number and slenderness ratio of an elliptical shape using potential theory and the Pohlhausen method (11:499). The effect of pressure gradient is then modeled by determining if a pressure minimum exists between the forward stagnation point and the computed transition location based on Reynolds number. If such a pressure minimum exists, transition is assumed to occur at the earlier upstream point of minimum pressure.

Drag results using this transition criteria will tend to be somewhat higher than would be found experimentally. The point of boundary-layer instability usually is a short distance upstream of the transition location (11:505). In addition, the magnitude of the pressure gradient is ignored and only the effect of adverse pressure gradient in causing earlier upstream boundary-layer transition is taken into account. The effect of a favorable pressure gradient in prolonging laminar flow has also been ignored. As a result, the computed boundary layers over the airfoil surface may be more turbulent in character than found experimentally, resulting in increased drag.

Grid

The grid topology used in this study is a conventional O-grid, with the grid cut line extending from the airfoil nose to the outer boundary. The grid was generated using the

interactive grid-generation program INGRID (6), developed at the Arnold Engineering Development Center (AEDC). Using this program, an algebraic grid was first constructed to obtain the desired point distribution and then refined using an elliptic smoother to obtain a more orthogonal grid. The characteristics of the grid used in this study were based upon a limited sensitivity study of the effect of grid resolution on the computational solution along with the requirement of reasonable computer run times.

The outer boundary of the grid used in this study is circular and is located 14 airfoil chords from the airfoil surface. The size of the grid is 176 points in the wrap-around direction with 80 points in the normal direction. These points are clustered in areas of the grid where large flowfield gradients exist such as the boundary layer, near the airfoil nose, the jet slot and over the Coanda surface. A portion of the grid displaying the airfoil and the grid point spacing is shown in Figure 4. Figure 5 shows the jet slot region and the Coanda surface.

One difficulty in using the O-grid topology on circulation airfoil geometries is apparent in Figure 6. Due to sharp corners in the airfoil contour at the slot exit, a high degree of grid skewness is unavoidable. The effect caused by the lack of grid orthogonality and the resulting poor grid transformation metrics in the slot region on the computational results is unknown.

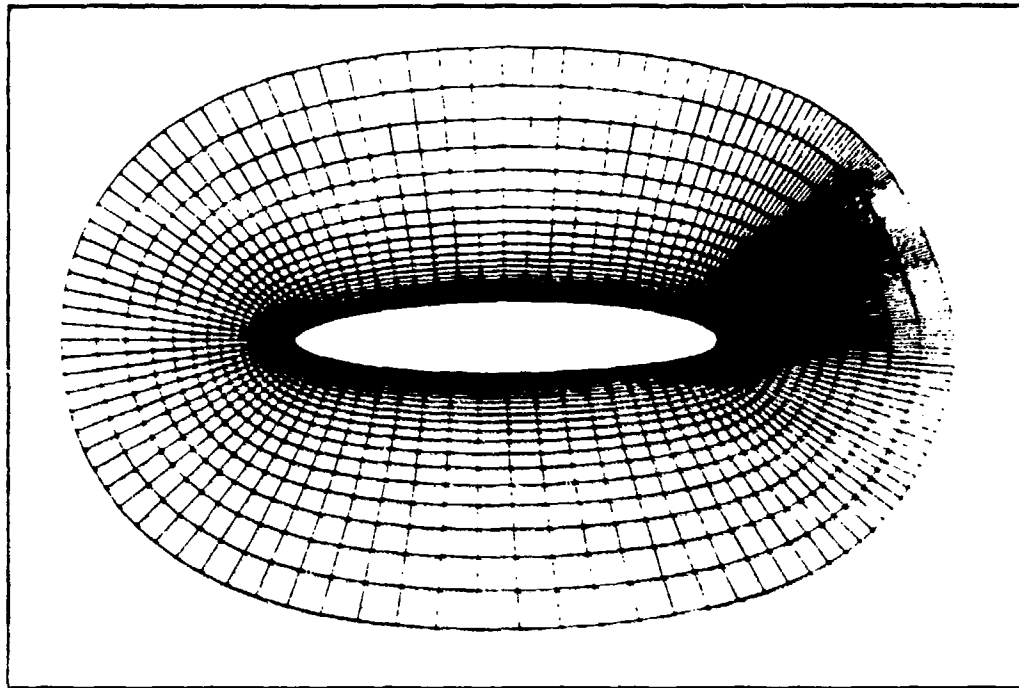


Figure 4. Interior Region of Airfoil Computational Grid

Computer Resources

Two different types of computers were used to solve the Navier-Stokes equations used in this study. Most results were obtained on a Floating Point Systems M64-20 Minisupercomputer. This 64-bit precision computer has 32 megabytes (MB) of memory and performs at a speed of 6 million floating point operations per second (MFLOPS). This machine is capable of parallel processing and able to take advantage of the vectorizable fortran code of the Navier-Stokes method. A Digital Equipment Corporation VAXstation III/GPX Workstation was also used to obtain solutions in this study. This 32-bit precision computer

has 8 MB of memory and an execution speed of approximately 2 MFLOPS. Both of these computers are representative of the type of computers that most aircraft design groups have easy access to in the United States.

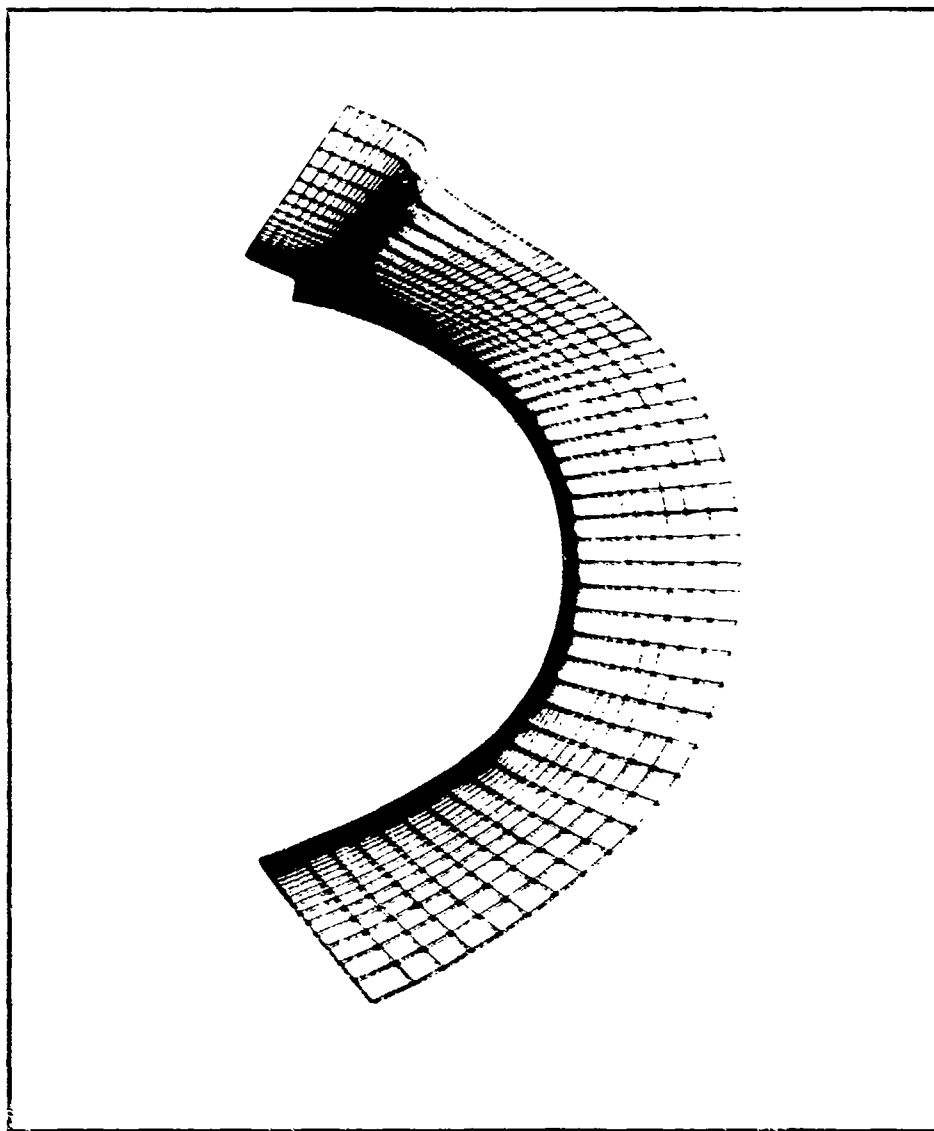


Figure 5. Jet Slot and Coanda Surface Region of Airfoil Computational Grid

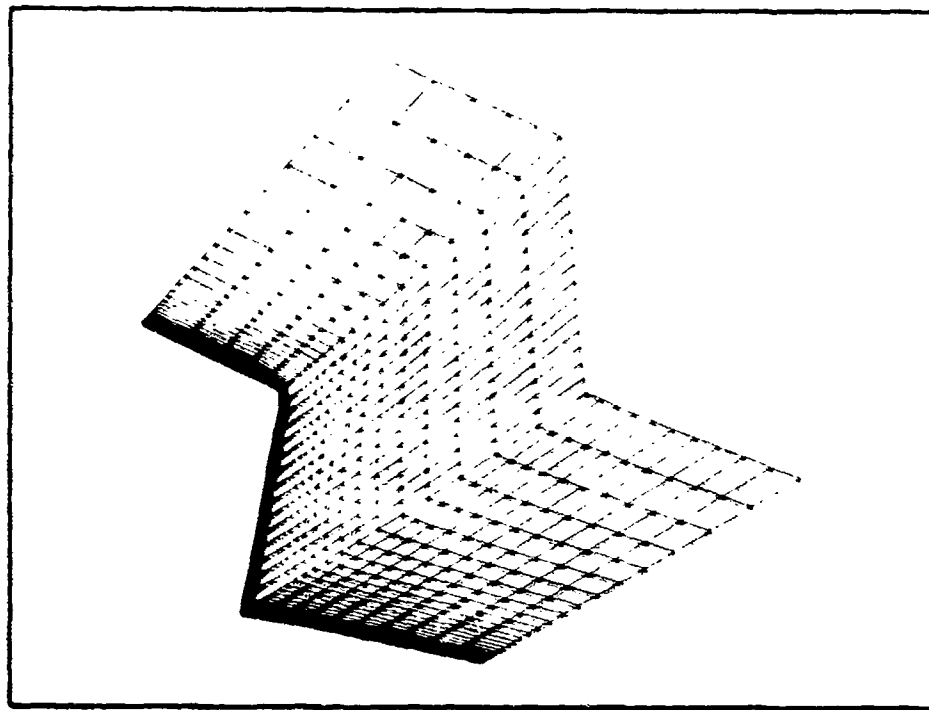


Figure 6. Close-up of Slot Region of Airfoil Computational Grid

III. Results and Discussion

103RE Airfoil

The airfoil chosen for analysis in this study is the 103RE airfoil. This airfoil was designed at the David Taylor Naval Ship Research and Development Center (DTNSRDC) for application as a circulation control helicopter rotor. The 103RE airfoil is typical of circulation control airfoils and shown in Figure 7. The airfoil contour is a modified ellipse with a maximum camber of 1% chord located at 70% chord and has a reduced leading-edge radius. The airfoil maximum thickness is 16% chord. The jet nozzle is convergent with the jet slot located at 96.88% chord. The Coanda surface is a reduced ellipse with the radius of curvature varying from 4.6% chord at the slot to 2.8% chord at the airfoil trailing edge. The airfoil coordinates for both upper and lower surfaces are provided in the Appendix.

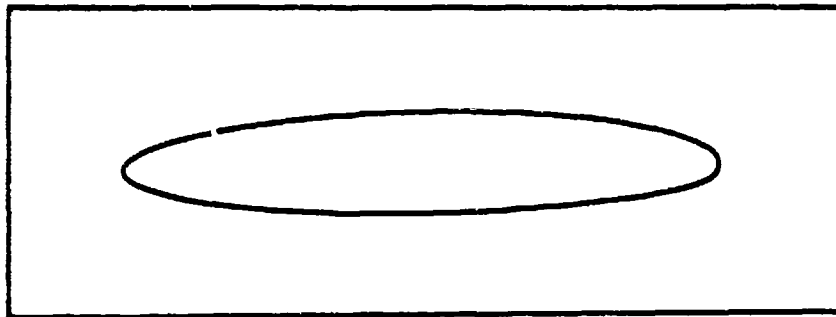


Figure 7. 103RE Circulation Control Airfoil Geometry

One of the reasons this airfoil was chosen for analysis is due to the extensive wind-tunnel data available. The DTNSRDC in 1982 conducted a comprehensive transonic wind-tunnel evaluation of various circulation control airfoils including the 103RE airfoil (1). The purpose of the wind-tunnel evaluation was to expand the circulation control airfoil database and to learn more about the effects of transonic flow on these airfoils. This DTNSRDC test is the source of all experimental data used in this study.

Solutions were obtained by applying the computational Navier-Stokes method at the experimental wind-tunnel test conditions shown in Table 1. Throughout the remainder of this study, the computational and experimental results obtained at the conditions shown in Table 1 will be referred to using the wind-tunnel "Point" number nomenclature. All runs in the wind

Table 1. 103RE Airfoil Computational and Experimental Test Conditions

| Point | M_∞ | $R_e (X10^{-6})$ | α_{eff} (deg) | P_t/P_∞ | T_t/T_∞ | $(C_L)_{WT}$ | $(C_L)_{NS}$ |
|-------|------------|------------------|----------------------|----------------|----------------|--------------|--------------|
| 33 | 0.30 | 3.12 | -0.25 | 1.000 | 1.000 | 0.0009 | 0.0000 |
| 35 | 0.30 | 3.11 | -0.92 | 1.137 | 0.956 | 0.0094 | 0.0096 |
| 36 | 0.30 | 3.09 | -1.66 | 1.204 | 0.934 | 0.0179 | 0.0187 |
| 38 | 0.30 | 3.06 | -2.45 | 1.573 | 0.905 | 0.0322 | 0.0332 |

tunnel were performed at a geometric angle of attack of zero degrees. However, due to interference from the tunnel walls, an angle-of-attack correction was applied as shown in Table 1. Experimental values of lift and pitching moment were obtained by

integrating the pressure distribution from pressure taps located on the airfoil. Experimental drag values were obtained using a wake probe.

Choosing the airfoil jet slot height to use for the computational study was complicated because the wind-tunnel test model jet slot would expand when pressurized. Since the slot height is directly proportional to the jet mass flow rate, this provided difficulties in matching the experimentally determined blowing coefficient. The wind-tunnel test apparatus had a rigid jet slot height of 0.0020 chord. However, upon pressurization of the jet plenum chamber, DTNSRDC estimates that the actual slot heights were in the range of 0.0021-0.0023 chord for the conditions shown in Table 1. A slot height of 0.0023 chord was used in this study for all Navier-Stokes runs with blowing. Figure 8 shows a correlation of computed versus experimentally measured blowing coefficient. The solid line represents an exact correlation. As Figure 8 shows, the computed values of blowing coefficient tended to be slightly greater than those found experimentally. All computed values were found to be within 5% of experiment.

Force and Moment Comparison

Plotted in Figure 9 is the airfoil lift coefficient versus blowing coefficient. This figure illustrates the large increases in lift that are possible with circulation control airfoils. Lift coefficients on the order of 2 and even higher are possible. The addition of even moderate amounts of blowing

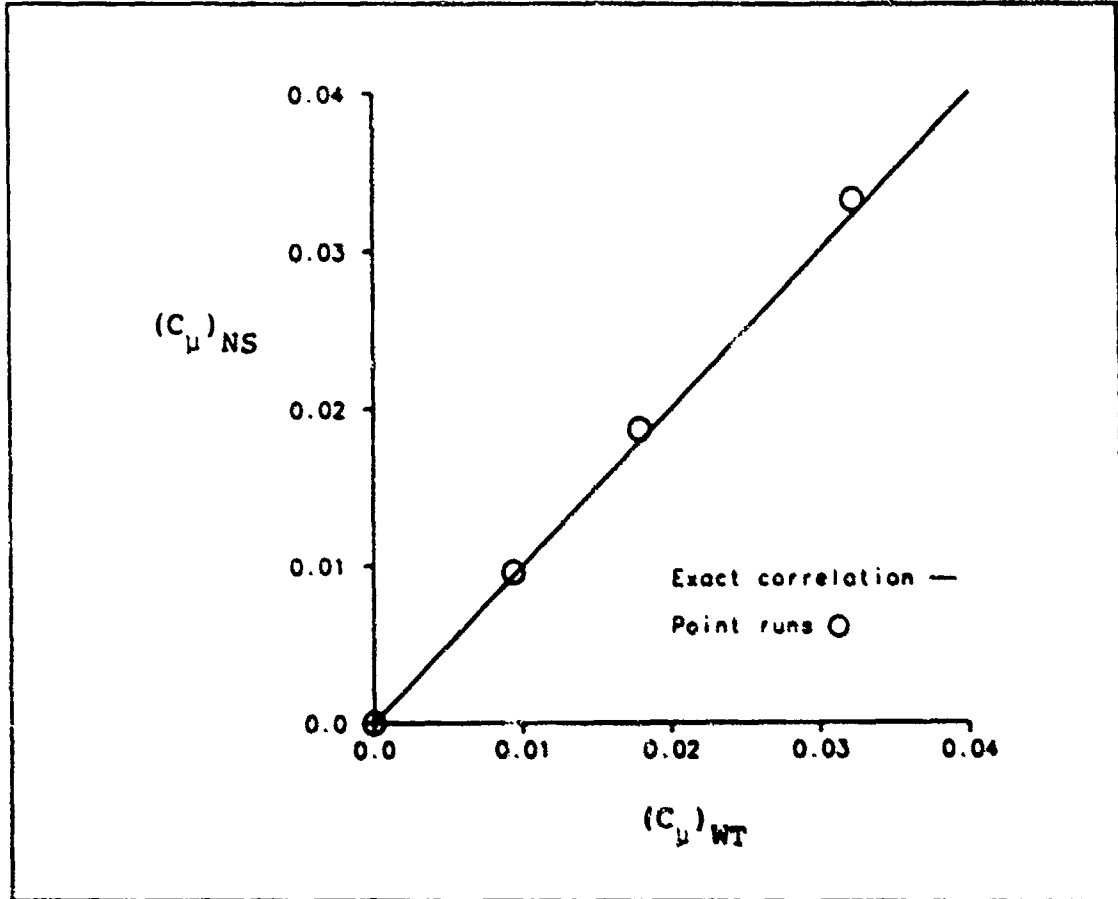


Figure 8. Correlation of Computational and Experimental Blowing Coefficients

is a powerful mechanism for substantial increases in airfoil performance. Overall, the computed and experimental solutions show reasonable agreement with a relatively constant difference in lift coefficient across the range of blowing coefficients. The slopes of the computational and experimental solutions, which are a measure of blowing efficiency in generating lift, are in very close agreement.

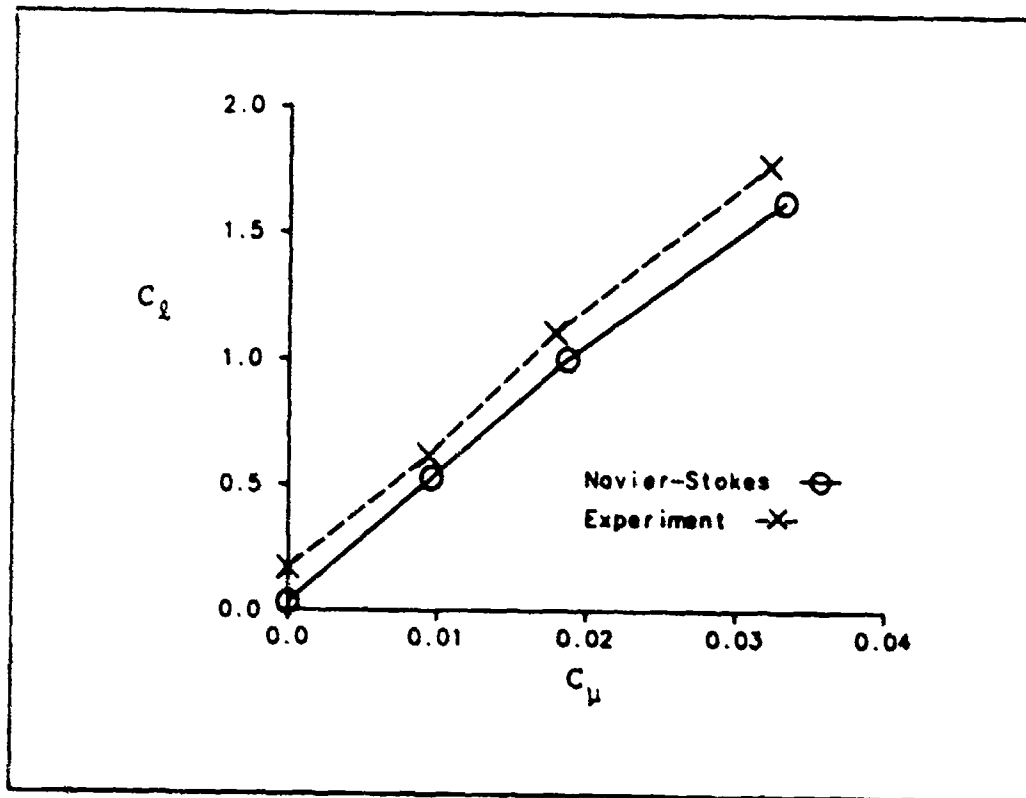


Figure 9. Variation of Computational and Experimental Lift Coefficient with Blowing Coefficient

Differences in the magnitudes of the experimentally observed and computed values of lift can be attributed to the turbulence model. Evidently, the use of the generic curvature constant from Eq (27) causes premature detachment of the jet boundary layer from the Coanda surface, resulting in decreased lift when compared with experiment. This result is reasonable considering that the magnitude of the empirical curvature correction constant controls the degree of turbulent transport within the boundary layer over the Coanda surface. The resulting stability of the boundary layer plays a great role in determining how far downstream the boundary layer will remain

attached in the influence of a significant adverse pressure gradient (11:220).

It is interesting to note in Figure 9 that the lift decrement between the computational and experimental results is nearly constant regardless of the jet blowing coefficient. Using a similar empirical curvature correction, Pulliam has shown that the curvature constant is essentially dependent only on the type of airfoil Coanda surface and freestream Mach number (10:144). Thus, for a constant value of the empirical curvature term, one would expect the lift results to be independent of blowing coefficient.

Figure 10 compares the computational and experimental pitching moment variation with blowing coefficient. This plot shows that as the airfoil blowing coefficient is increased, the nose down pitching moment of the airfoil also increases. The agreement between the computational and experimental results is very good. This is partially due to the fact that the large amount of suction on the Coanda surface, coupled with a long moment arm, tends to dominate the pitching moment calculation. The pitching moment data show that one problem with generating large lift with circulation control airfoils is that a large pitching moment is also produced. To maintain aircraft trim, this moment would need to be countered by another control surface.

The variation of drag coefficient with blowing coefficient is shown in Figure 11. Although the computational and experimental data appear to offer similar trends, the agreement

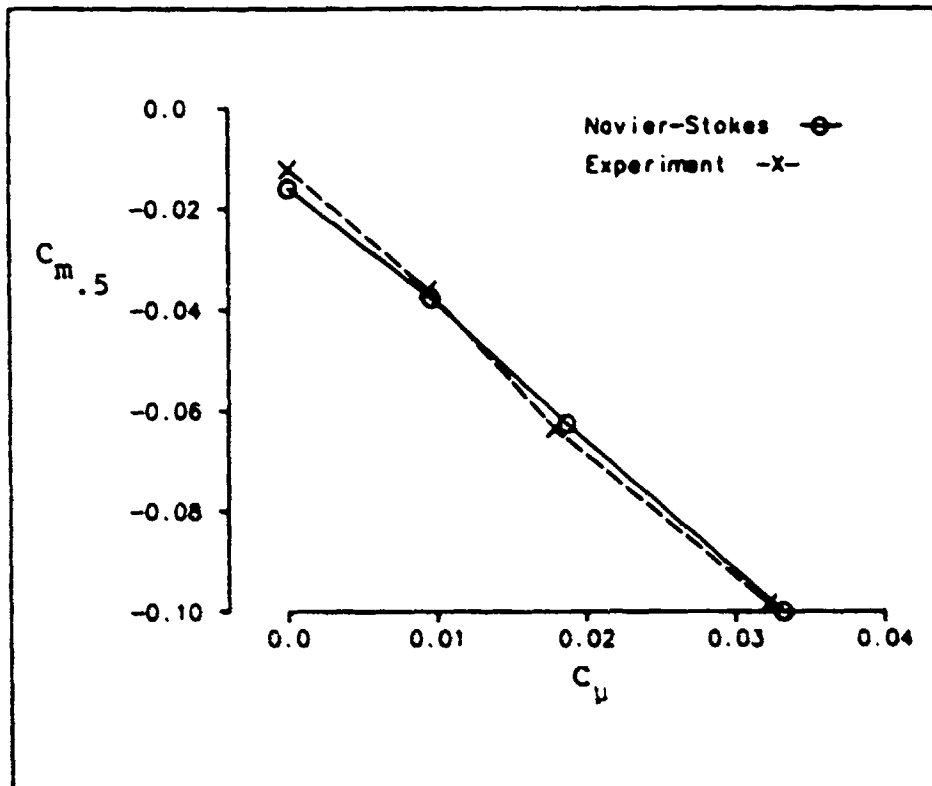


Figure 10. Variation of Computational and Experimental Pitching Moment Coefficient with Blowing Coefficient

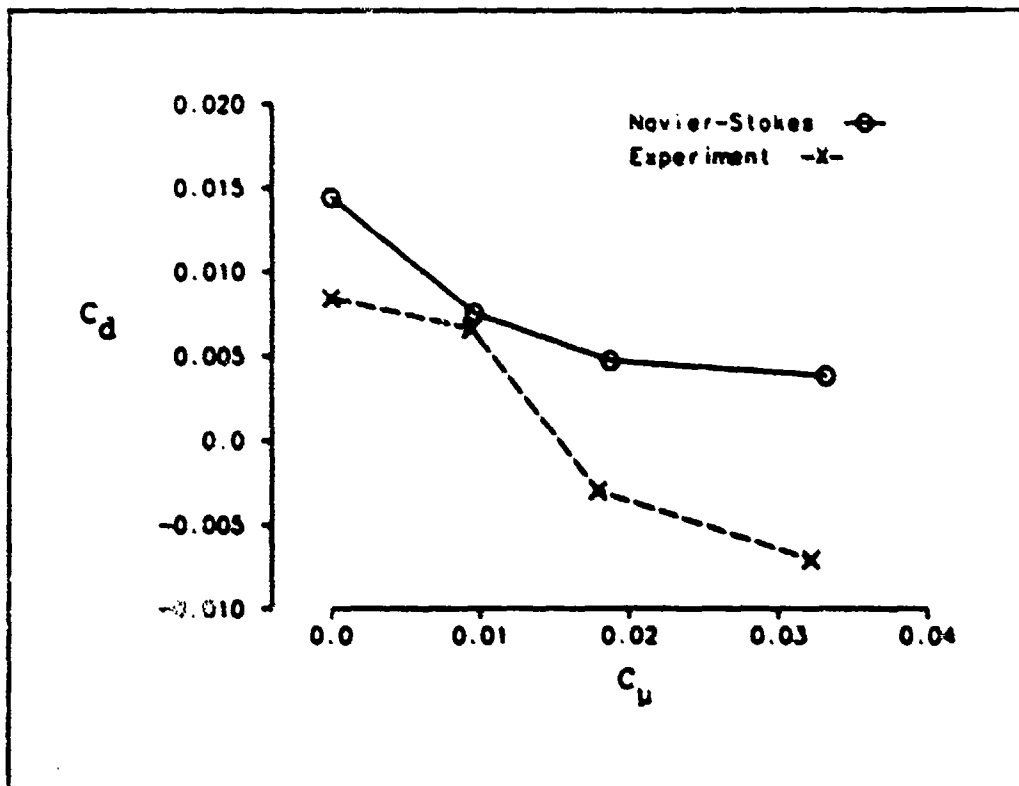


Figure 11. Variation of Computational and Experimental Drag Coefficient with Blowing Coefficient

is somewhat disappointing. The cause for this lack of agreement could be due to a variety of reasons. One contributing factor is the conservative nature of the Navier-Stokes turbulence model transition criteria. The transition criteria used in this study will tend to overpredict the level of airfoil drag coefficient due to its neglect of the influence of favorable pressure gradient on boundary-layer transition. Another contributing factor could be due to the inaccuracies of measuring airfoil drag in the wind tunnel with a wake probe. Some degree of uncertainty is sure to be present due to corrections that account for tunnel side wall interference and the upstream insertion of momentum from the jet slot. Unfortunately, the degree of this uncertainty is unknown.

Point 33 Results

Point 33 proved to be an interesting case even though no airfoil blowing was applied. One of the reasons for this is that the solution shows that inaccurate predictions of boundary-layer transition location can have a major impact on solution accuracy. Since no blowing is applied in this case, the large difference in airfoil drag coefficient shown in Figure 11 must be due to boundary-layer transition effects. From Figure 11, the computed value of drag coefficient is found to be about twice that measured in the wind tunnel. Thus, the computational method predicted a much further upstream transition location than actually existed experimentally. This conclusion was confirmed by using the computational method with

transition occurring much further downstream on the airfoil surface. Drag coefficient results were then found to be in much closer agreement with experiment.

Figure 12 compares the computed airfoil pressure coefficient distribution with that observed experimentally. The seemingly poor scale used in this figure is used in order to maintain a constant scale with the jet blowing results that follow. In this manner, the effect of different blowing coefficients on the overall airfoil pressure coefficient distribution can be compared directly for the different cases

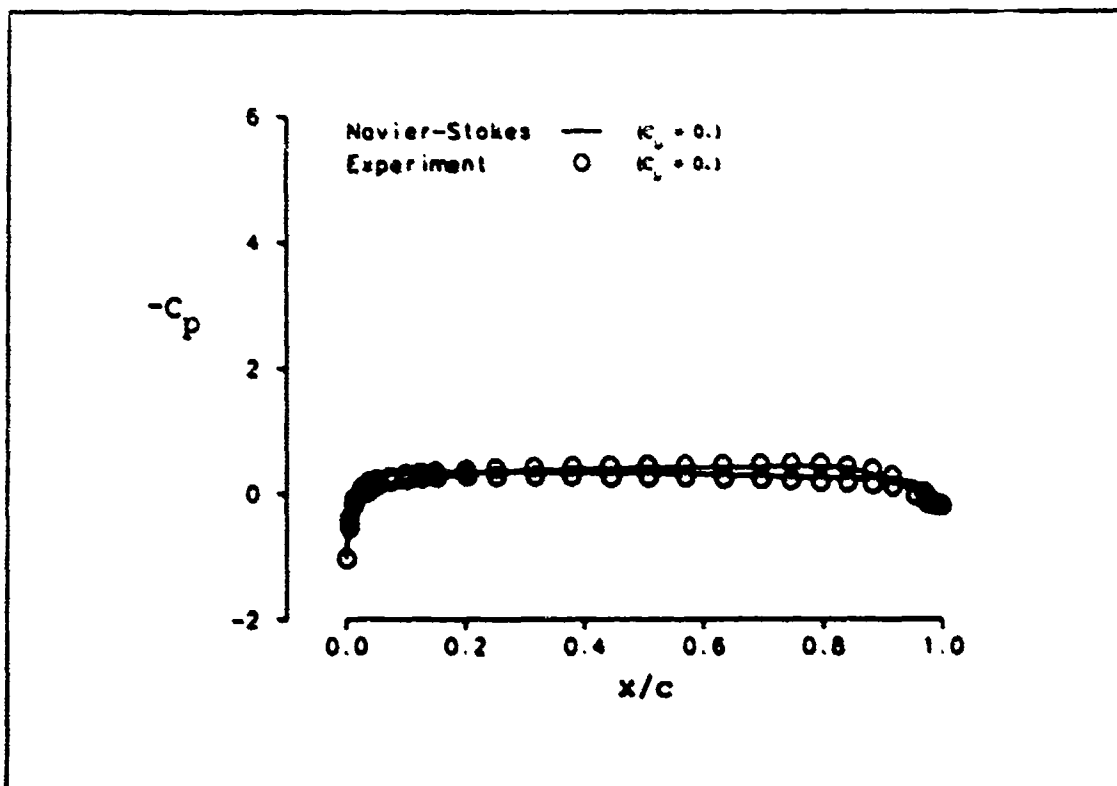


Figure 12. Computational and Experimental Pressure Coefficient Distributions (Point 33)

considered. The effect of the airfoil camber over the aft portion of the airfoil is apparent from Figure 12 in a slight pressure decrease over the upper surface in this region. Also note that a slightly favorable pressure gradient is encountered over a considerable portion of the airfoil upper surface. Since favorable pressure gradients tend to prolong laminar flows, this observation would support the hypothesis that considerable laminar flow is encountered in this case. A weak adverse pressure gradient is encountered over the airfoil lower surface until the Coanda surface is encountered. It is well known that adverse pressure gradients tend to promote laminar transition to a turbulent boundary layer. The lower surface pressure gradient is so small, however, that it probably has little effect on boundary-layer transition in this case.

Computed Mach contour solutions for the flowfield are shown in Figure 13 about the entire airfoil and in the vicinity of the Coanda surface in Figure 14. A maximum Mach number of 0.36 is found in the flowfield for the computed solution at a chordwise position of about 73% chord, just external to the airfoil boundary layer. In Figure 13, the stagnation point on the airfoil leading edge is clearly visible. In addition, the aft flow separation due to the blunt trailing edge of the airfoil is apparent in Figures 13 and 14.

Figure 15 shows the computed velocity solution in the airfoil trailing-edge region. The velocity solution in this region is represented by vectors with the arrow direction representing the local flow orientation and the arrow magnitude

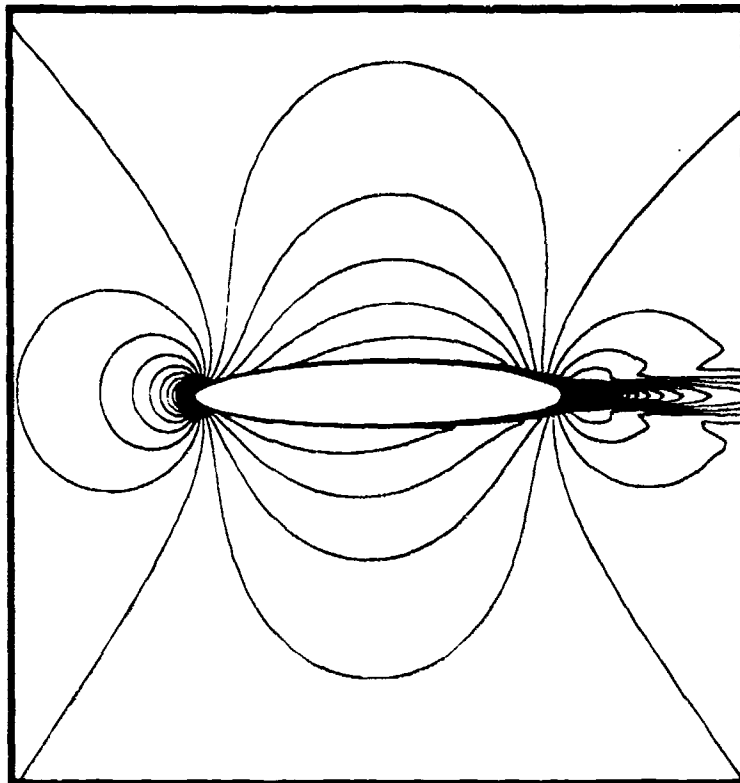


Figure 13. Airfoil Region Computational Mach Contours, $C_{\mu} = 0$ (Point 33)

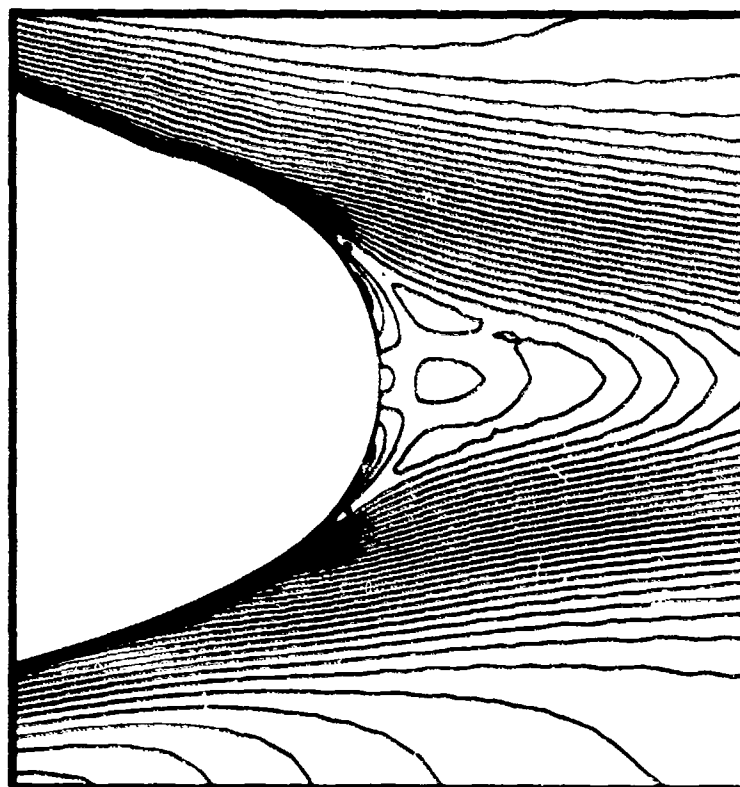


Figure 14. Coanda Surface Region Computational Mach Contours, $C_{\mu} = 0$ (Point 33)

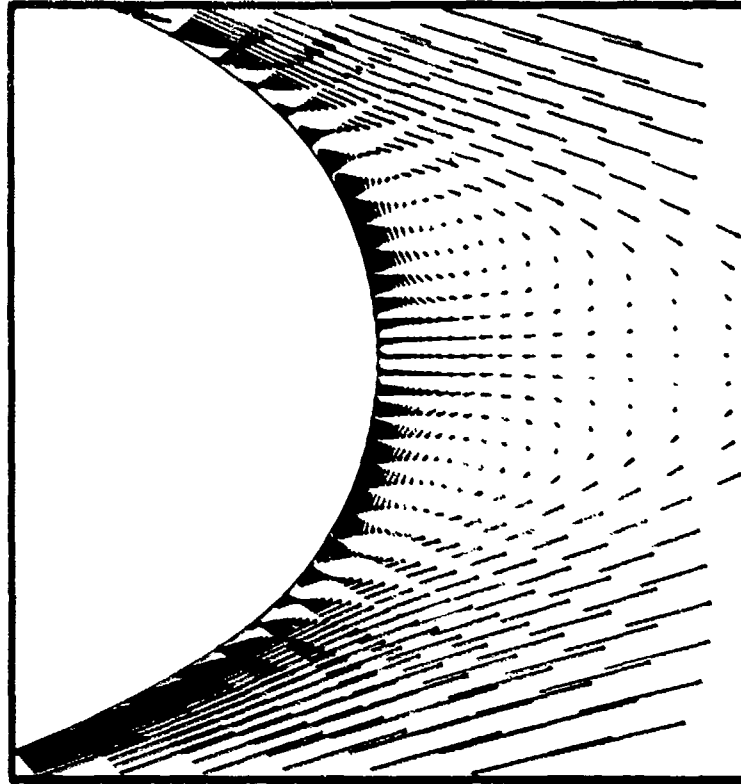


Figure 15. Coanda Surface Region Computational Velocity Vectors, $C_{\mu} = 0$ (Point 33)

representing the relative speed of the flow. The separation of the upper and lower surface boundary layers from the airfoil is readily apparent. In addition, the complicated flow in the base separation region appears to consist of two counter-rotating vortices. Note that the two vortices are nearly identical in size and are placed symmetrically about the airfoil chord for this flight condition.

Point 35 Results

Point 35 represents the first case with jet slot blowing. As shown in Figure 16, the addition of even a small amount of blowing has a noticeable effect on the airfoil pressure coefficient distribution. The most obvious characteristic of circulation control airfoil pressure distributions is the suction peak introduced over the airfoil Coanda surface due to the jet. This injected flow not only affects the aft pressure distribution, but also significantly alters the pressure distribution over the entire airfoil. Comparing Figures 12 and

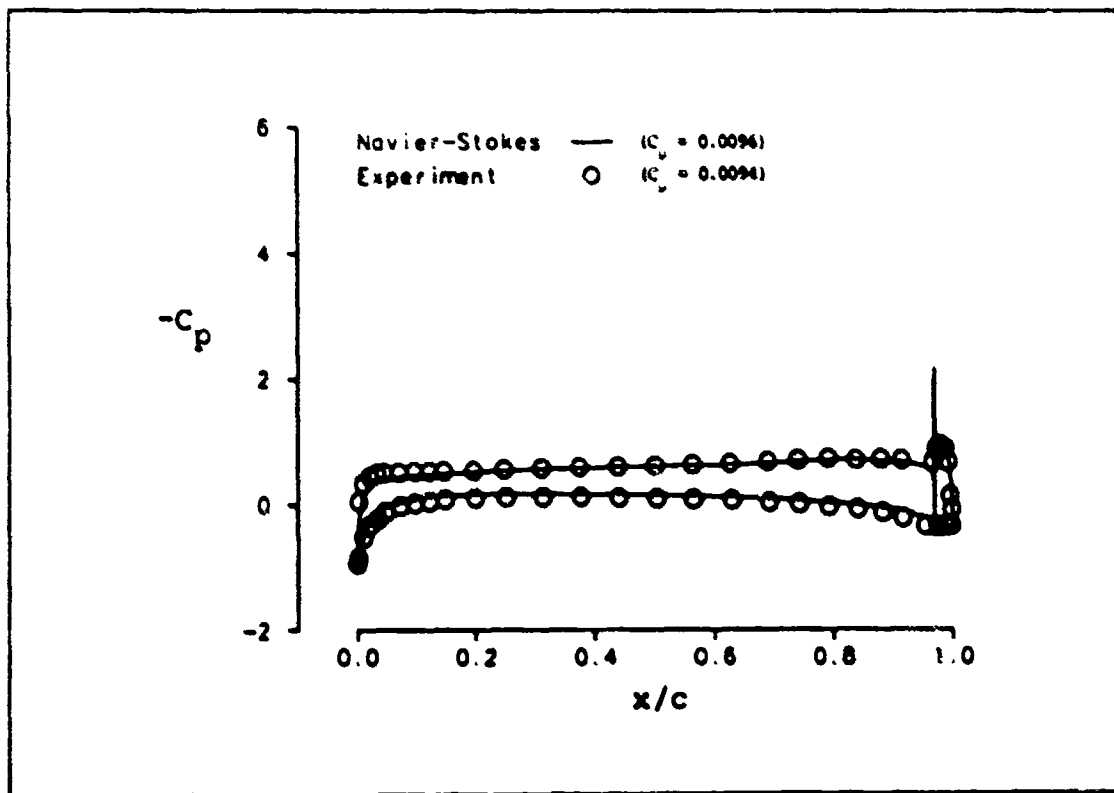


Figure 16. Computational and Experimental Pressure Coefficient Distributions (Point 35)

16 confirms this fact. Strictly speaking, at such a low value of blowing coefficient, the jet slot blowing acts more like a boundary-layer control device than circulation control. Note that a favorable pressure gradient is maintained over the airfoil upper surface until about 80% chord and that a weak adverse pressure gradient is encountered on the lower surface from about 30% to 90% chord. Comparing the computed and experimental pressure distributions, overall agreement is found to be good. The computed pressure distribution appears to have most difficulty matching the experimental pressure distribution in the airfoil upper leading-edge and lower trailing-edge regions.

The effect of blowing on the surrounding flowfield is shown in Figures 17 and 18. In Figure 17, the front stagnation point has moved toward the lower airfoil surface. In addition, the two trailing-edge separation points have also moved towards the lower surface. This movement of the stagnation points suggests increased circulation about the airfoil. Figure 18 shows the influence of the jet about the Coanda surface. The Coanda effect is clearly illustrated by the tangential injection of the jet and resulting attachment of the jet to the Coanda surface. A maximum Mach number of 0.53, located at the center of the jet slot exit, is encountered in the computed flowfield for this case.

The entrainment of the flowfield by the jet blowing is shown in Figure 19. Also note the prolonged attachment of the boundary layer on the upper surface. As for Point 33, two

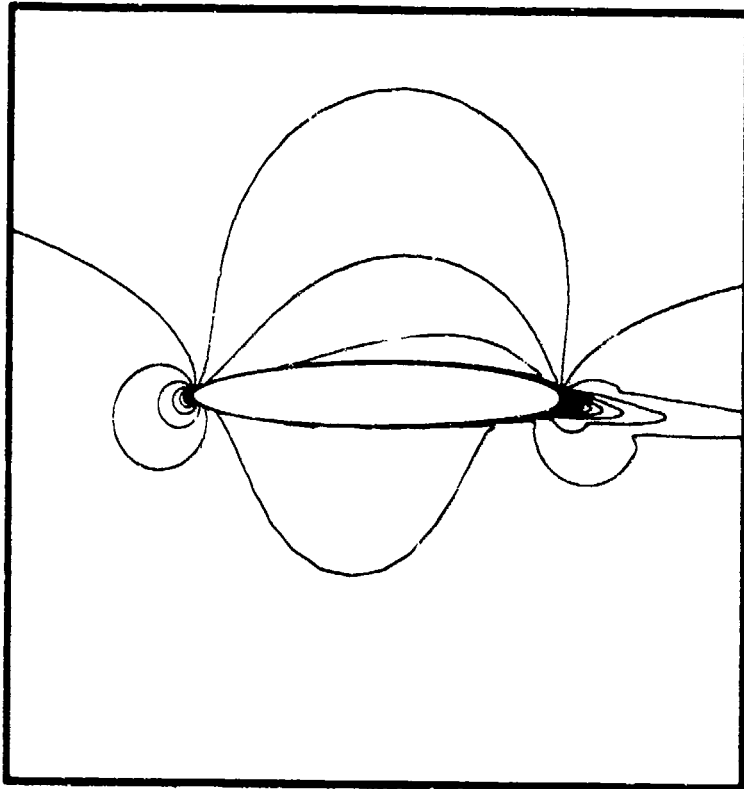


Figure 17. Airfoil Region Computational Mach Contours,
 $C_{\mu} = 0.0096$ (Point 35)

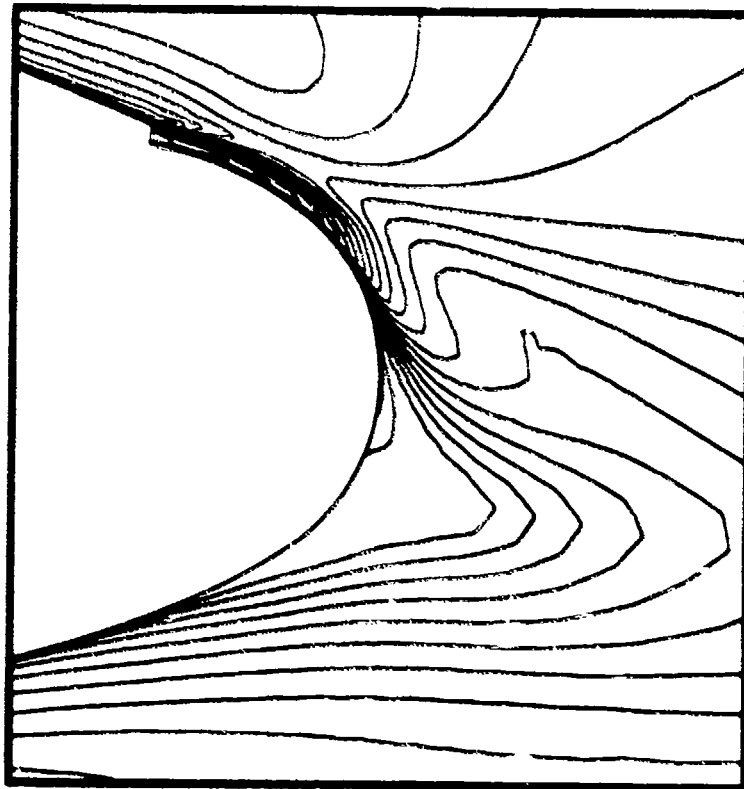


Figure 18. Coanda Surface Region Computational Mach Contours,
 $C_{\mu} = 0.0096$ (Point 35)

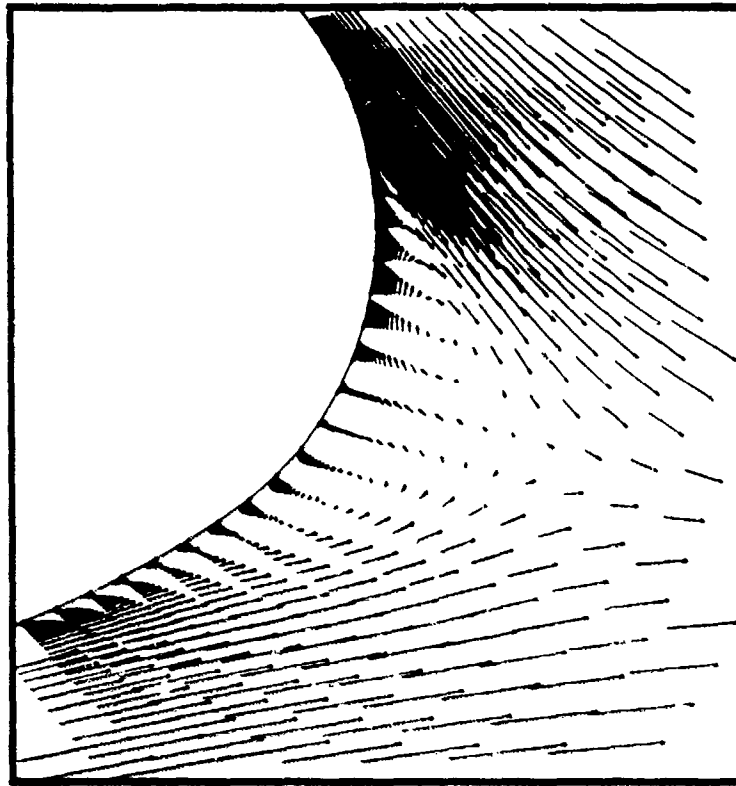


Figure 19. Coanda Surface Region Computational Velocity Vectors, $C_{\mu} = 0.0096$ (Point 35)

counter-rotating vortices exist in the separated region about the airfoil trailing edge, however, the vortices have been displaced toward the lower surface due to the jet blowing.

Point 36. Results

The pressure coefficient distribution for this case is shown in Figure 20. The level of blowing for this case is increased, being reflected in the resulting pressure distribution. Comparing Figures 16 and 20, it is apparent that

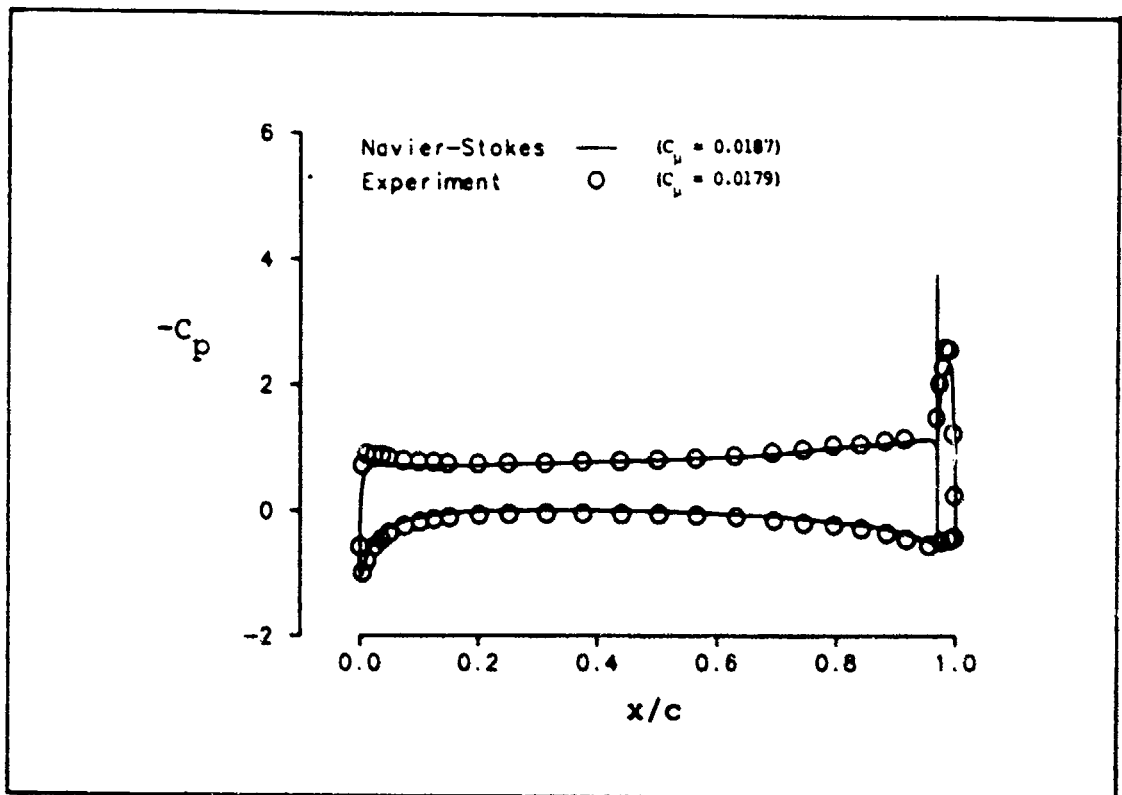


Figure 20. Computational and Experimental Pressure Coefficient Distributions (Point 36)

the suction peak over the Coanda surface has increased for Point 36, as well as the amount of leading-edge suction. A weak adverse pressure gradient is now encountered on the airfoil upper surface at about 3% chord and on the lower surface at about 35% chord. In comparing the computational and experimental pressure distributions, the Navier-Stokes method is underpredicting the amount of suction on the Coanda surface and airfoil leading edge.

Located near the middle of the jet slot exit, the computed maximum Mach number reached in the flowfield for this case is 0.75. As shown in Figure 21, the influence of additional blowing has resulted in further downward movement of the leading and trailing edge stagnation points indicating increased circulation. Figure 22 shows that the increased amount of blowing results in a stronger jet that is able to remain attached to the Coanda surface further downstream.

The velocity flowfield is illustrated in Figure 23. The increased jet blowing entrains the flowfield with increased

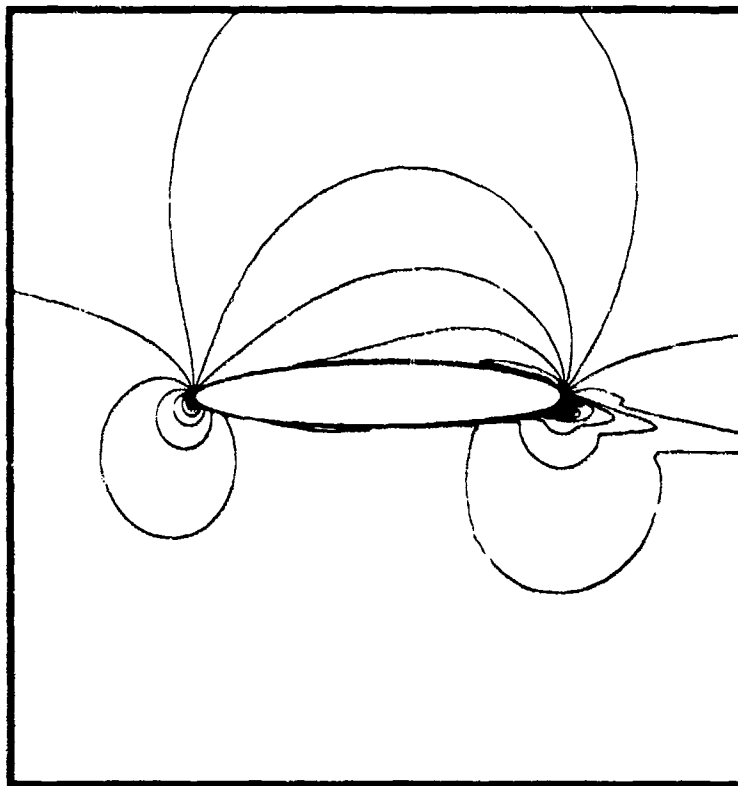


Figure 21. Airfoil Region Computational Mach Contours,
 $C_{\mu} = 0.0187$ (Point 36)

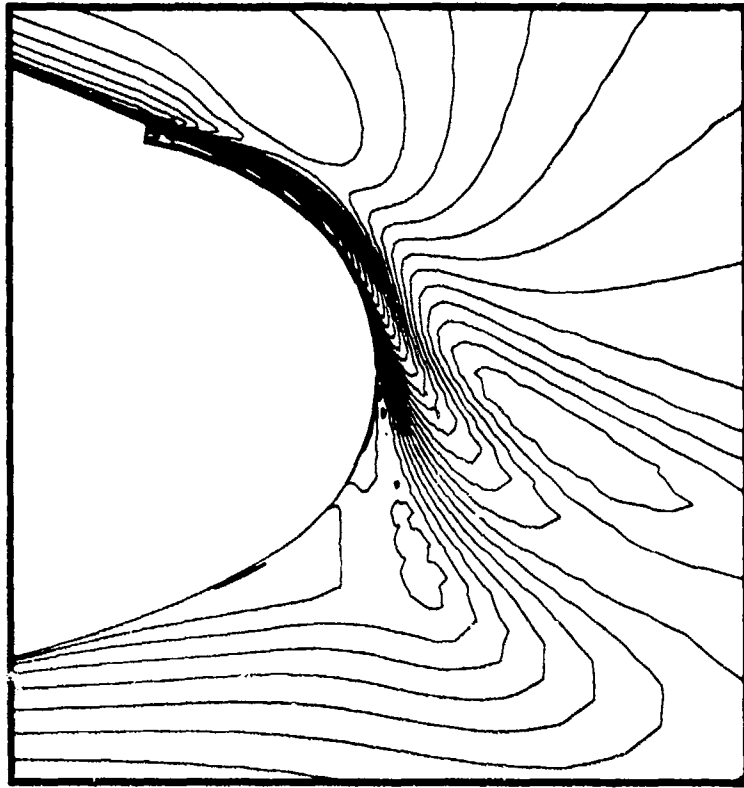


Figure 22. Coanda Surface Region Computational Mach Contours, $C_{\mu} = 0.0187$ (Point 36)

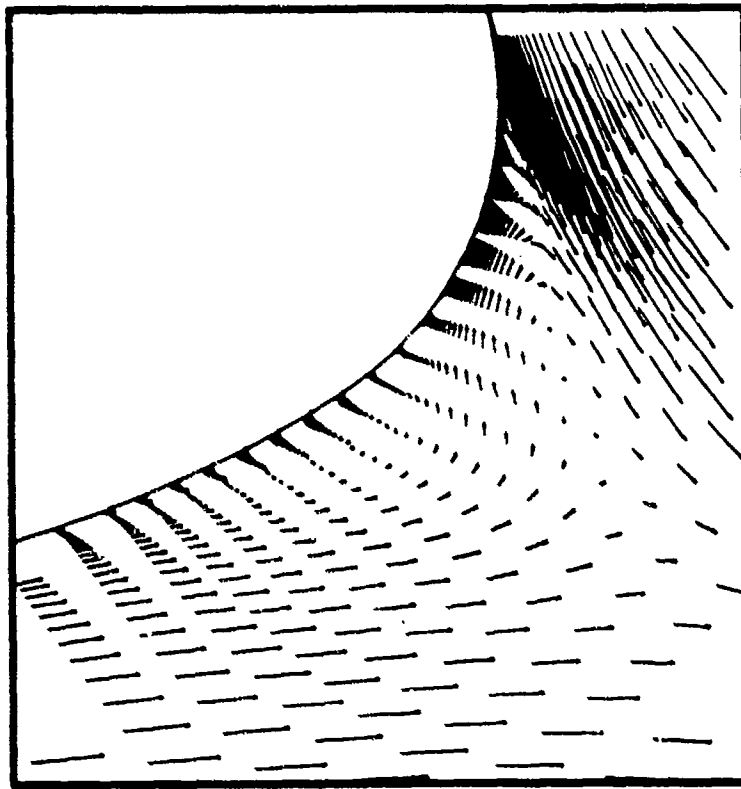


Figure 23. Coanda Surface Region Computational Velocity Vectors, $C_{\mu} = 0.0187$ (Point 36)

effectiveness. Unlike the lower blowing coefficient cases, the separated region now contains only one vortical structure. It appears that the jet boundary-layer detachment from the Coanda surface has sufficient strength to turn the lower boundary-layer flow without the formation of a second vortex. Also note that the remaining vortex has moved further towards the airfoil lower surface and now has a flattened shape.

Point 38 Results

The last case examined in this study was obtained at a moderately high blowing coefficient of about 0.03. The resulting pressure coefficient distributions from both experiment and computations are shown in Figure 24. Due to the increased amount of slot blowing, the amount of suction over the Coanda surface and leading edge has grown considerably. As a result, a strong adverse pressure gradient is encountered on the airfoil upper surface at about 2% chord. This pressure gradient is probably of sufficient strength to cause boundary-layer transition. Once again, the computational results underpredict the amount of suction on both the airfoil leading edge and Coanda surface.

Point 36 is the first case in which a region of local supersonic flow is encountered in the flowfield. This region is near the jet slot exit and Coanda surface junction with the Mach number reaching 1.13. Hence, at a freestream Mach number of 0.3, a transonic flow now exists over the airfoil due to the high jet blowing coefficient. Figure 25 shows the significant

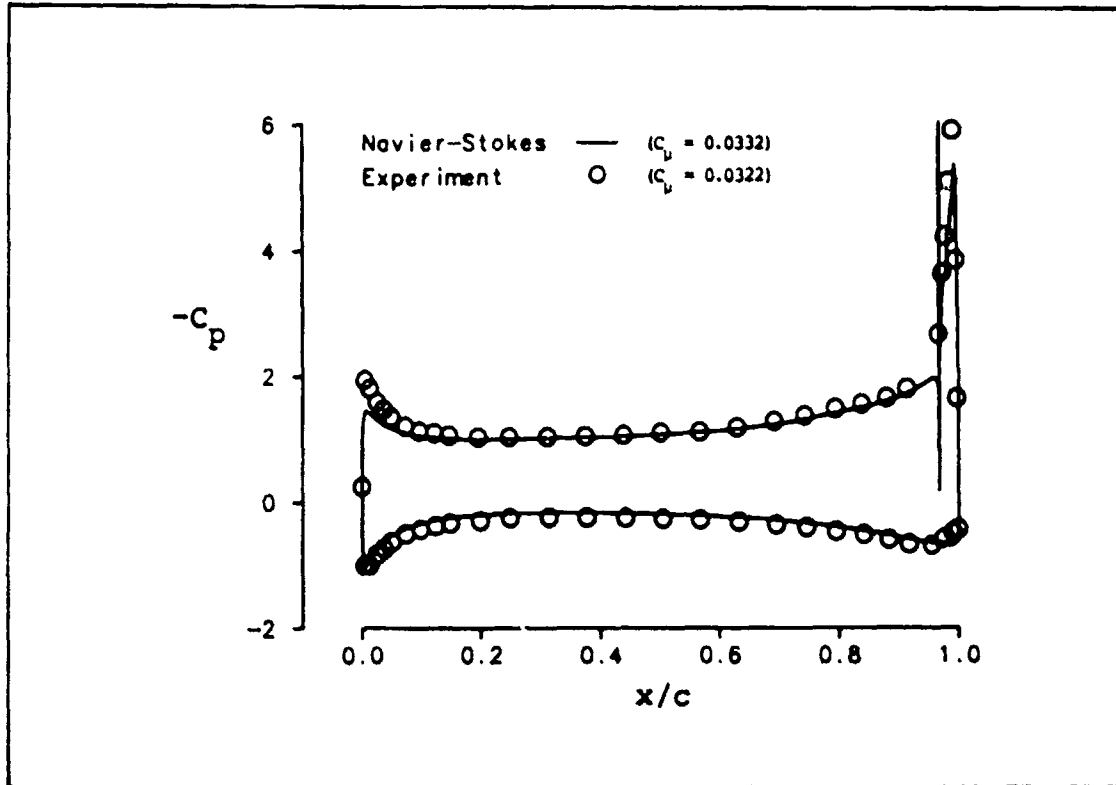


Figure 24. Computational and Experimental Pressure Coefficient Distributions (Point 38)

movement of the leading and trailing edge stagnation points toward the lower airfoil surface. Figure 26 illustrates the jet remaining attached further downstream along the Coanda surface and turning through approximately 90 degrees.

The velocity flowfield shown in Figure 27 is similar to that found for Point 36 except that the jet detaches further downstream along the Coanda surface and is of greater strength. Once again, only one flattened vortex is present and it is displaced further down on the airfoil lower surface.

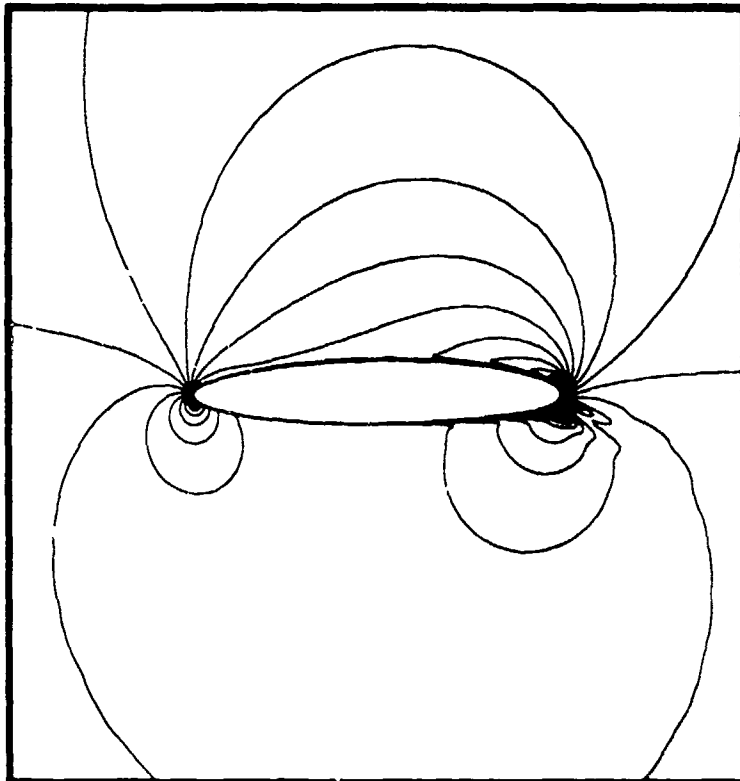


Figure 25. Airfoil Region Computational Mach Contours,
 $C_\mu = 0.0332$ (Point 38)

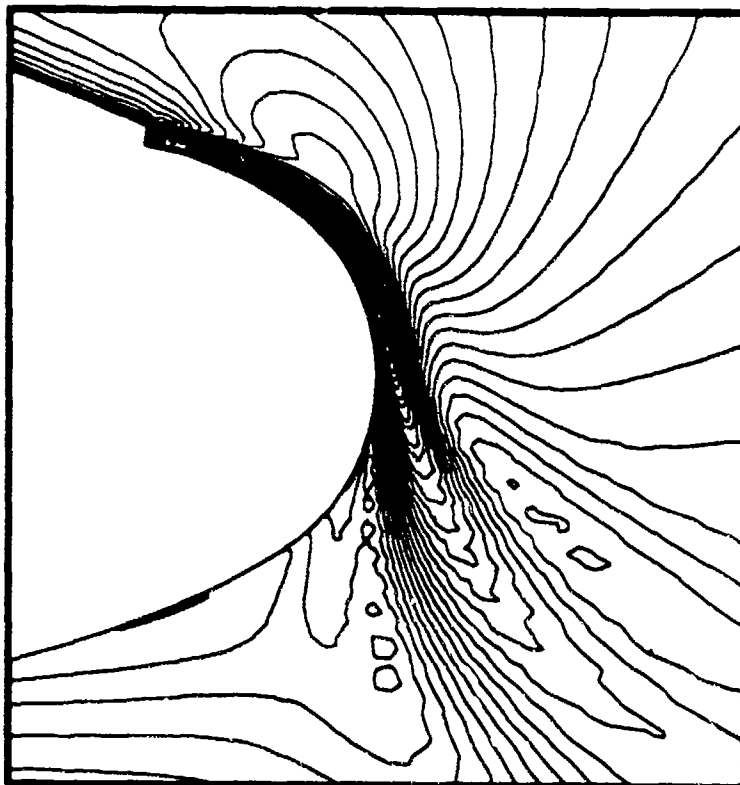


Figure 26. Coanda Surface Region Computational Mach Contours,
 $C_\mu = 0.0332$ (Point 38)

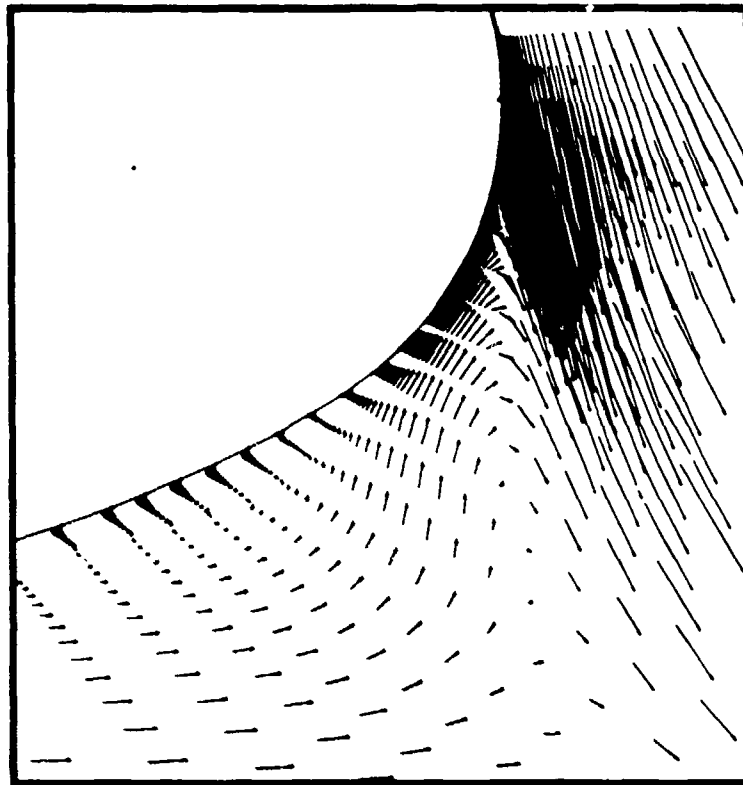


Figure 27. Coanda Surface Region Computational Velocity Vectors, $C_u = 0.0332$ (Point 38)

Computed Jet Characteristics

Shown in Figure 28 are the computed jet velocity profiles at the slot exit for Points 35, 36 and 38. As expected, the velocity of the jet increases with increasing blowing coefficient. The profiles are very similar in nature with the possible exception of Point 38. Due to the high jet total pressure ratio for this case, the jet becomes partially choked at the slot exit. This is reflected in the flattening of the velocity profile.

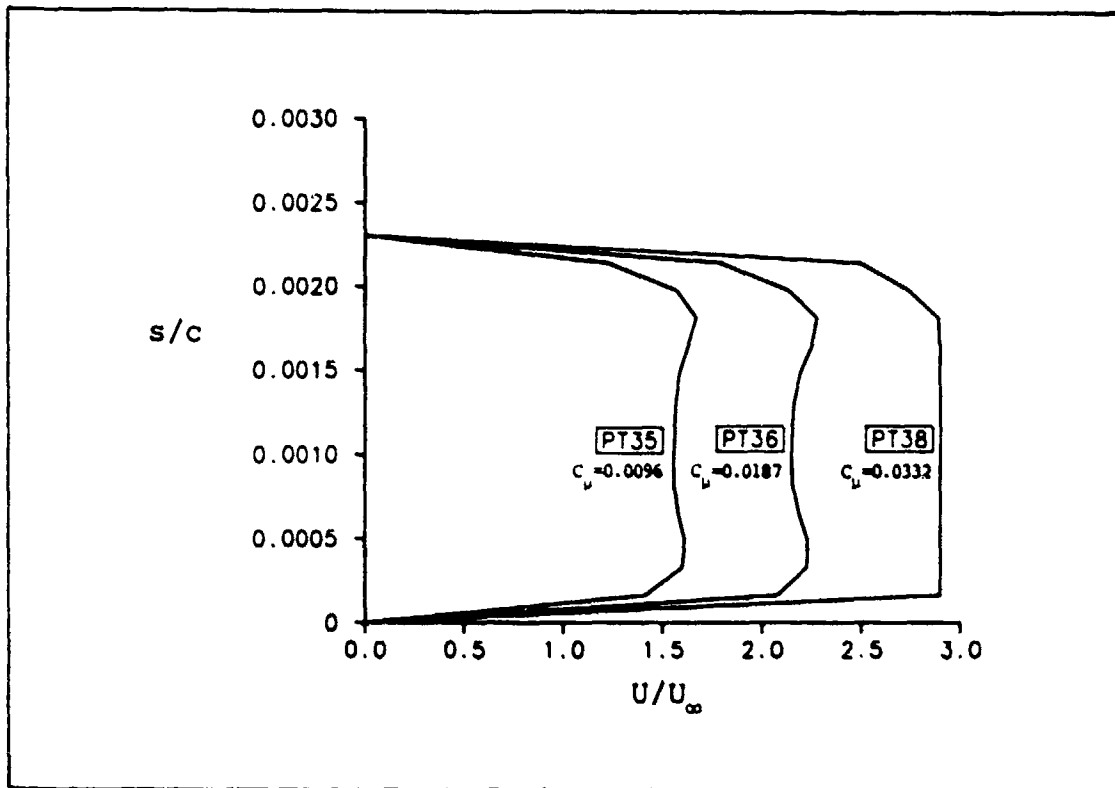


Figure 28. Variation of Computational Jet Slot Exit Velocity Profiles with Blowing Coefficient

Figure 29 illustrates the effect of jet blowing coefficient on the jet boundary-layer detachment point. As the amount of jet blowing is increased, the jet boundary layer remains attached to the Coanda surface further downstream and is turned through a greater angle. For the highest blowing coefficient case shown in Figure 29, the Coanda effect is readily apparent as the flow is turned through approximately 90 degrees and separates at the airfoil trailing edge.

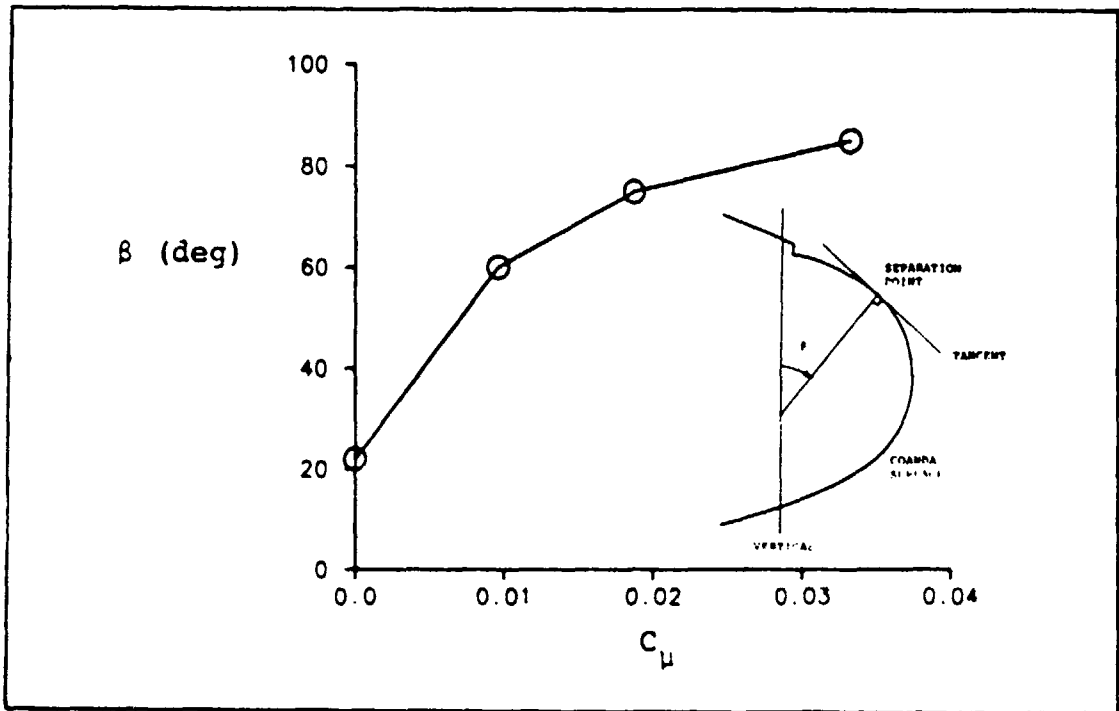


Figure 29. Variation of Computational Jet Detachment Point with Blowing Coefficient

Solution Sensitivity to Curvature Constant

It appears from the previous discussion concerning Figure 9 that use of the generic curvature constant given in Eq (27) provides premature jet boundary-layer detachment from the Coanda surface, resulting in lower values of airfoil lift coefficient than that found experimentally. In this section an attempt is made to determine how dependent the computational solution is upon the turbulence model curvature correction constant. Using

Point 38, which is the highest blowing coefficient case examined in this study, several Navier-Stokes solutions are obtained by varying the empirical curvature constant from 1 to 10. In addition, the value of curvature constant that best matches the experimental value of lift is also determined and the resulting pressure coefficient distribution is compared with experiment.

The sensitivity of lift coefficient with curvature correction is shown in Figure 30. The computed lift coefficient varies from about 1.5 to 2.0 depending on the value of curvature constant. Lift coefficients up to 11% too high or 15% too low

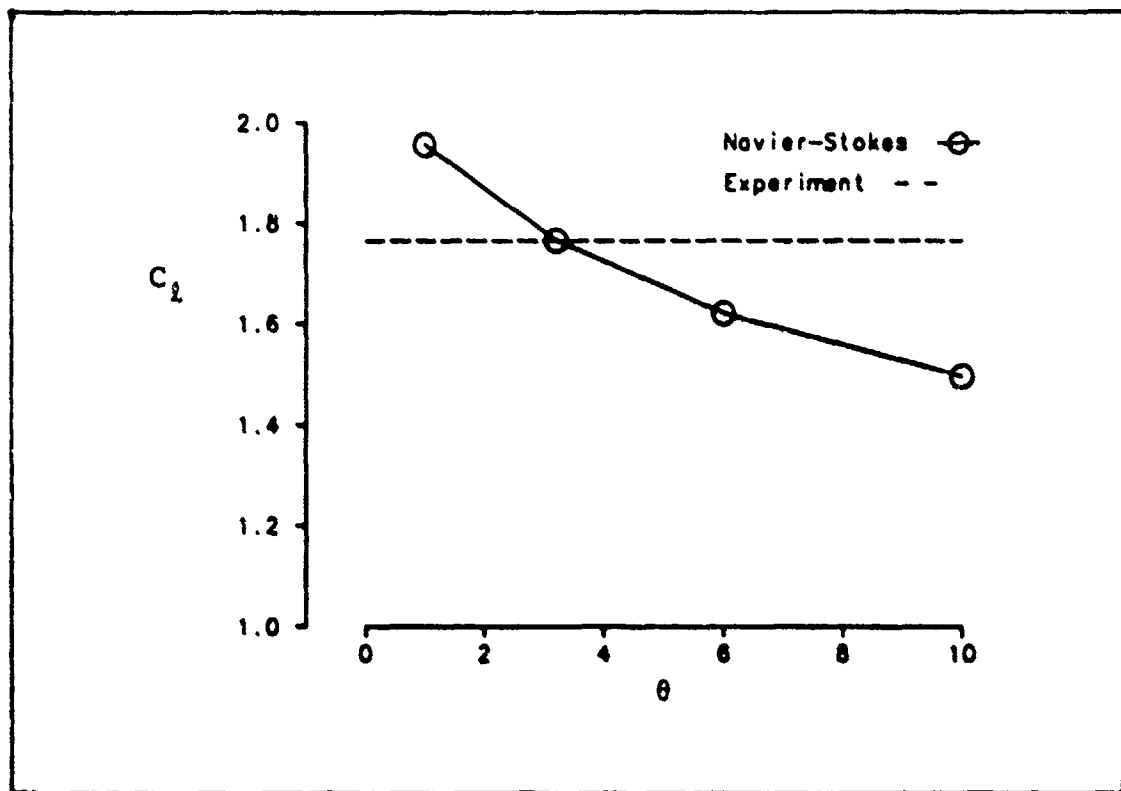


Figure 30. Variation of Computational Lift Coefficient with Curvature Constant (Point 38)

compared with the experimental results could be found computationally depending on the choice of curvature constant used. It is apparent for this airfoil and flight condition that the generic curvature constant value of 6 from Eq (27), used for the earlier computational predictions, is too large. For this case, a curvature constant of about 3.2 will provide a computed value of lift coefficient that is approximately equal to that found experimentally.

Figure 31 shows the sensitivity of the pitching moment results to the curvature constant. Depending on the curvature constant used, pitching moment varies from about 0% to -6% of the experimentally measured value. Thus, airfoil pitching moment does not appear to be strongly driven by the choice of curvature constant.

The drag coefficient sensitivity to curvature constant is displayed in Figure 32. The experimental value of drag coefficient for Point 38 is -0.0071. The computed values of drag coefficient vary from 0.0099 to 0.0019. Drag coefficient appears to be more strongly driven by curvature constant than pitching moment. Using a value of curvature constant optimized for lift coefficient, however, does not help the drag correlation.

The resulting pressure coefficient distribution using the "matched" curvature constant value of 3.2 is shown compared with the experimental distribution in Figure 33. Overall, the correlation is very good. The computed Coanda surface suction pressures compare well with the experimental data, obtaining a

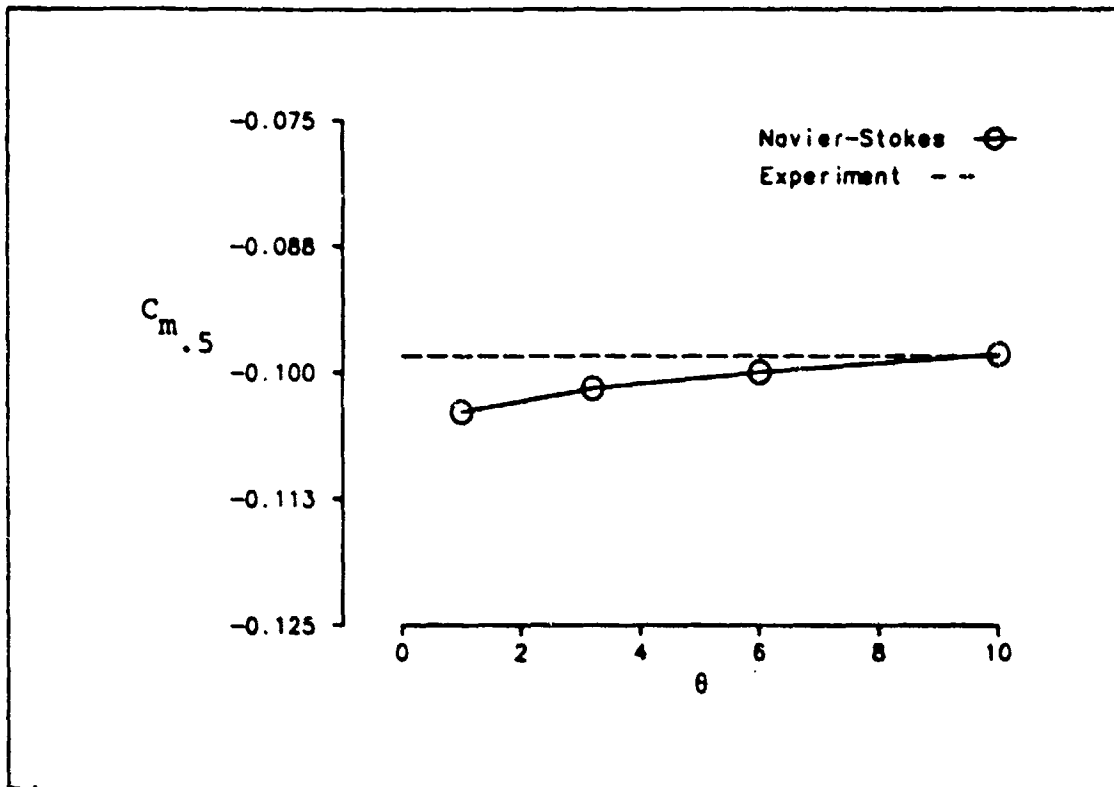


Figure 31. Variation of Computational Pitching Moment Coefficient with Curvature Constant (Point 38)

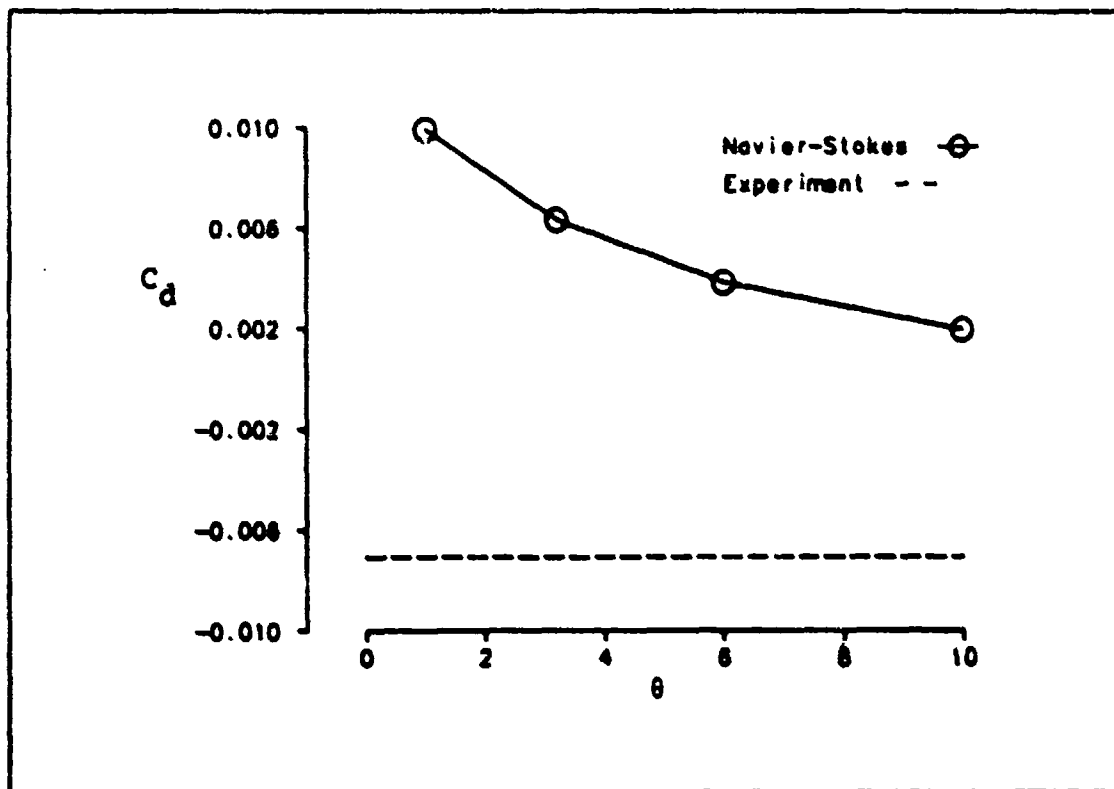


Figure 32. Variation of Computational Drag Coefficient with Curvature Constant (Point 38)

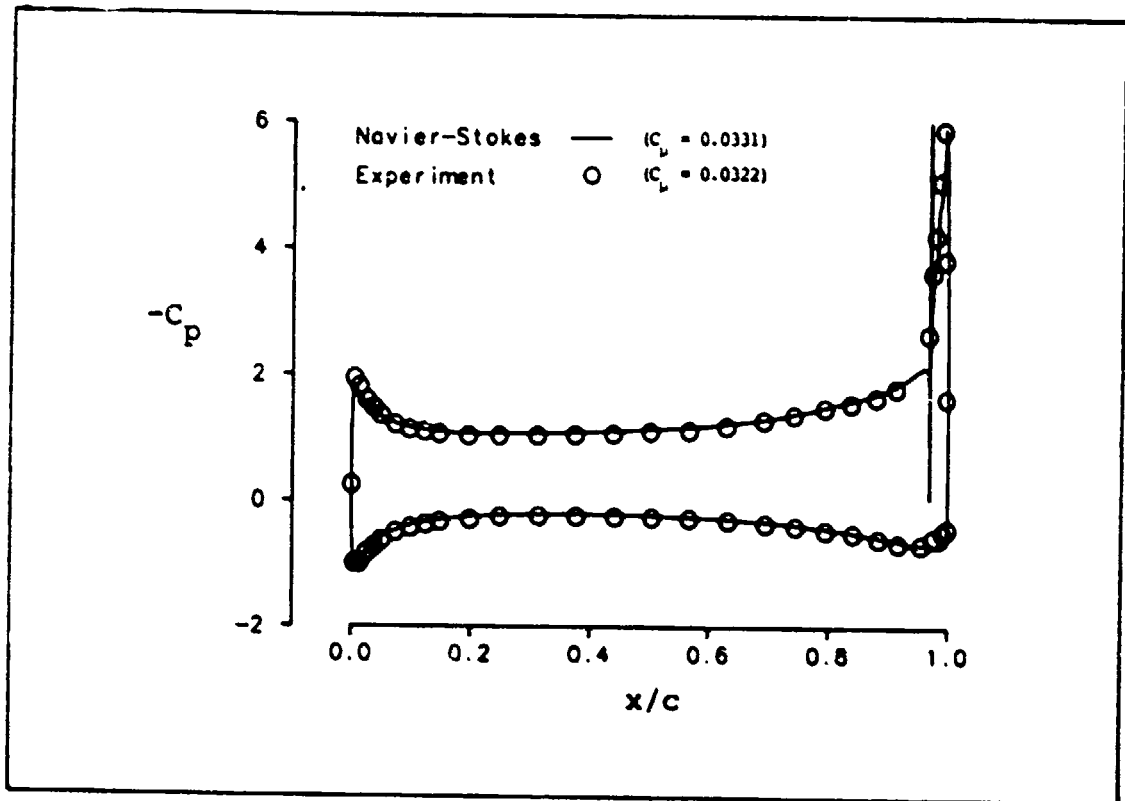


Figure 33. Computational and Experimental Pressure Coefficient Distributions, $\theta = 3.2$ (Point 38)

good match of the suction peak. Some weaknesses in the computational solution appear at the airfoil upper leading-edge suction and trailing-edge separation regions. The differences in the upper leading-edge suction region may be due to the small difference between the computational and experimental blowing coefficients.

Pulliam et al. (10) has also computed the solution for Point 38 using his Navier-Stokes method and obtained very good agreement with the experimental data. The same difficulty in

predicting the pressure coefficient distribution in the airfoil trailing-edge region was discovered, although his agreement in the upper leading-edge region was superior, possibly due to a better match of the computational and experimental blowing coefficient. It would be interesting to compare the value of turbulence model curvature correction constant used by Pulliam with the value found in this study. However, even though his turbulence model correction is similar to the one used in this study, a direct comparison of curvature correction constants is not possible due to the different formulations used (10:143).

Shrewsbury observed a similar difficulty in predicting pressure coefficient in the airfoil trailing-edge region with a different circulation control airfoil (13:6). This discrepancy could be due to a weakness of the turbulence model in simulating the separated flow region. Shrewsbury used a turbulence model curvature correction constant of 25 in his paper (13:3). However, the circulation control airfoil used in his study was a research model and not similar to the 103RE airfoil used in this study. Differences in the Coanda surface as well as flight condition simulated could account for the variation in curvature constants used.

Use of the Method in a Design Environment

Use of the computational Navier-Stokes method has demonstrated that relatively accurate predictions of circulation control airfoil lift coefficient and pitching moment coefficient are possible. Using the generic curvature correction constant

from Eq (27), both the computed lift and pitching moment results for the blowing cases were found to be within 15% of the experimental values. Although the computational results were somewhat sensitive, this same result remained true even for different values of the turbulence model curvature constant. Based upon these results, use of the computational method for circulation control airfoil design purposes appears promising. The effect on aerodynamic performance of different airfoil parameters such as jet slot height, jet slot position and Coanda surface curvature at different blowing coefficient, Mach number and angle-of-attack conditions could be determined using such a method.

Unfortunately, computational solutions of the Navier-Stokes equations require a great commitment of resources and time. Construction of a suitable flowfield grid about the airfoil of interest is both time consuming and manpower intensive. Considerable computer resources are required to obtain converged solutions. Once a flowfield solution has been computed it needs to be interpreted. These drawbacks are even more acute in a design environment where parametric studies are performed and quick job turnaround is required.

However, due to the complex non-linear behavior of circulation control flowfields, airfoil designers are being driven to use Navier-Stokes methods. Fortunately, due to the great increases in computer speed and memory in the last ten years, these methods are becoming more practical to use. No longer is the use of a CRAY or other large mainframe computer

required to solve complex problems using the Navier-Stokes equations in two-dimensions.

All of the Navier-Stokes solutions obtained in this study were performed on either a Floating Point Systems M64-20 or Digital Equipment Corporation VAXstation III/GPX. The amount of central processing unit (CPU) time required to obtain solutions using the computational method for both of these computers is summarized in Table 2. Convergence of the airfoil forces and moment to a steady-state value was typically on the order of 1500 iterations. As can be seen in Table 2, the amount of time required to perform one job is very large. It is obvious that using the method for quick parametric evaluations is not possible using these computers. However, this method could be used to build a database of information from which empirical relations could be devised for parametric studies.

Table 2. Typical Navier-Stokes Run Times on Different Computers

| Computer | DPR | Time(hrs) |
|-------------|----------------------|-----------|
| DEC GPX | 3.9×10^{-3} | 23.40 |
| FPS M64-20 | 1.5×10^{-3} | 9.00 |
| CRAY XMP-12 | 2.5×10^{-5} | 0.15 |

Notes:

- (1) DPR: Data processing rate CPU sec/[(grid point)(iteration)]
- (2) Calculations based on 176 X 80 grid and 1500 iterations

Also shown in Table 2 is the CRAY CPU time for the method. Note that the use of such a high-speed computer greatly decreases job turnaround and makes the use of Navier-Stokes methods more practical for design. As increasingly capable computers are developed and made more accessible to the general engineering community, the potential for using the Navier-Stokes equations for design purposes will continue to increase.

IV. Conclusions

The two-dimensional compressible mass-averaged Navier-Stokes equations have been solved for a typical circulation control airfoil using the implicit approximate-factorization algorithm of Beam-Warming and turbulence model of Baldwin-Lomax with a curvature correction due to Bradshaw. This study is unique in that the predictive capability of the computational method is explored by examining the importance of the empirical Bradshaw curvature correction constant. This was accomplished by first using a generic value of curvature constant at various blowing coefficients and then checking the sensitivity of the computational results to various curvature constant values at one blowing coefficient.

Strengths of the computational method using the generic curvature constant included an accurate prediction of the airfoil pitching moment and lift curve slope due to blowing when compared with experiment. Predicted levels of airfoil lift coefficient, although reasonable, were found to be consistently low when compared with experiment due to the generic curvature constant providing premature jet detachment from the Coanda surface at various jet blowing coefficients. Computed and measured airfoil drag results followed the same trends, but the lack of overall drag coefficient agreement was somewhat disappointing.

Lift coefficient was found to be quite sensitive, pitching moment not sensitive, and drag coefficient moderately sensitive to the value of curvature constant used. The value of curvature constant required for the computational lift coefficient to match that found experimentally was also determined for the highest blowing coefficient case considered. Using the experimentally correlated curvature constant, the computational and experimental pressure distributions compared very well, except in the leading-edge suction and trailing-edge separation regions.

In spite of the sensitivity of the computational results to the Bradshaw curvature correction constant, the method provided relatively accurate predictions of airfoil performance for the circulation control airfoil used in this study. Based on this result, the computational method shows promise as a design tool. The effects of different circulation control design parameters such as airfoil jet slot height, jet slot position and Coanda surface curvature at different jet blowing coefficient, Mach number and angle-of-attack conditions could be explored using this method. Unfortunately, use of the method does not lend itself to quick parametric evaluations due to the large amount of resources and time required to obtain solutions. However, as increasingly capable computers are developed and made more accessible to the general engineering community, the potential for using computational solutions of the Navier-Stokes equations for design purposes will continue to increase.

V. Recommendations

Based upon the results of this study, the following recommendations for future research are made.

1. Compute solutions of other circulation control airfoils using the developed Navier-Stokes method. Using the generic curvature correction constant suggested by Bradshaw, compare the computational results with experimental data.
2. Using available wind-tunnel data on different circulation control airfoils at various flight conditions, determine the correlated value of curvature constant for each case. Attempt to develop an empirical correlation to provide the curvature constant from the Coanda surface geometry characteristics and flight condition of the airfoil.
3. Using available experimental data, examine the capability of the developed Navier-Stokes method to predict airfoil design sensitivities. Investigate the ability of the method to predict the effect of varying jet slot height, jet slot location, and multiple slots.
4. Explore the ability of the Navier-Stokes method to predict the compressibility stall of circulation control airfoils.
5. Develop an improved turbulence model without the need for an empirical constant by conducting experiments with wall-jet flows over convex curvature shapes.

Appendix: 103RE Airfoil Coordinates



Slot Height = 0.0023c

| <u>Upper Surface</u> | | <u>Lower Surface</u> | |
|----------------------|----------|----------------------|-----------|
| x/c | y/c | x/c | y/c |
| 0.000000 | 0.000000 | 0.000000 | 0.000000 |
| 0.000052 | 0.001021 | 0.000073 | -0.001019 |
| 0.000227 | 0.002119 | 0.000271 | -0.002113 |
| 0.000527 | 0.003247 | 0.000594 | -0.003236 |
| 0.000951 | 0.004397 | 0.001043 | -0.004376 |
| 0.001499 | 0.005562 | 0.001615 | -0.005529 |
| 0.002171 | 0.006739 | 0.002313 | -0.006692 |
| 0.002966 | 0.007926 | 0.003134 | -0.007862 |
| 0.003886 | 0.009122 | 0.004080 | -0.009038 |
| 0.004929 | 0.010324 | 0.005149 | -0.010217 |
| 0.006095 | 0.011532 | 0.006342 | -0.011400 |
| 0.007384 | 0.012744 | 0.007659 | -0.012584 |
| 0.008795 | 0.013961 | 0.009098 | -0.013770 |
| 0.010328 | 0.015180 | 0.010661 | -0.014955 |
| 0.011983 | 0.016402 | 0.012346 | -0.016140 |
| 0.013760 | 0.017626 | 0.014153 | -0.017323 |
| 0.015656 | 0.018851 | 0.016081 | -0.018505 |
| 0.017674 | 0.020076 | 0.018131 | -0.019684 |
| 0.019811 | 0.021302 | 0.020301 | -0.020860 |
| 0.022068 | 0.022527 | 0.022591 | -0.022031 |
| 0.024442 | 0.023751 | 0.025001 | -0.023200 |
| 0.026936 | 0.024975 | 0.027530 | -0.024362 |
| 0.029546 | 0.026196 | 0.030177 | -0.025520 |
| 0.032274 | 0.027415 | 0.032942 | -0.026672 |
| 0.035117 | 0.028632 | 0.035824 | -0.027817 |
| 0.038075 | 0.029845 | 0.038823 | -0.028955 |
| 0.041149 | 0.031056 | 0.041937 | -0.030087 |
| 0.044336 | 0.032263 | 0.045166 | -0.031210 |
| 0.047636 | 0.033465 | 0.048510 | -0.032325 |
| 0.051048 | 0.034664 | 0.051966 | -0.033432 |
| 0.054571 | 0.035857 | 0.055536 | -0.034529 |
| 0.058205 | 0.037046 | 0.059217 | -0.035617 |
| 0.061949 | 0.038230 | 0.063008 | -0.036694 |

Upper SurfaceLower Surface

| x/c | y/c | x/c | y/c |
|----------|----------|----------|-----------|
| 0.065801 | 0.039408 | 0.066910 | -0.037762 |
| 0.069760 | 0.040579 | 0.070920 | -0.038818 |
| 0.073827 | 0.041745 | 0.075039 | -0.039863 |
| 0.077999 | 0.042904 | 0.079264 | -0.040896 |
| 0.082275 | 0.044057 | 0.083595 | -0.041918 |
| 0.086655 | 0.045202 | 0.088031 | -0.042926 |
| 0.091137 | 0.046340 | 0.092571 | -0.043922 |
| 0.095721 | 0.047470 | 0.097214 | -0.044904 |
| 0.100404 | 0.048592 | 0.101958 | -0.045873 |
| 0.105187 | 0.049707 | 0.106802 | -0.046828 |
| 0.110068 | 0.050812 | 0.111746 | -0.047767 |
| 0.115045 | 0.051909 | 0.116787 | -0.048692 |
| 0.120117 | 0.052997 | 0.121925 | -0.049602 |
| 0.125283 | 0.054077 | 0.127159 | -0.050496 |
| 0.130543 | 0.055146 | 0.132487 | -0.051374 |
| 0.135894 | 0.056207 | 0.137907 | -0.052236 |
| 0.141334 | 0.057257 | 0.143420 | -0.053081 |
| 0.146864 | 0.058297 | 0.149022 | -0.053909 |
| 0.152481 | 0.059327 | 0.154713 | -0.054720 |
| 0.158185 | 0.060347 | 0.160491 | -0.055513 |
| 0.163973 | 0.061356 | 0.166356 | -0.056288 |
| 0.169844 | 0.062353 | 0.172304 | -0.057044 |
| 0.175797 | 0.063340 | 0.178336 | -0.057782 |
| 0.181831 | 0.064316 | 0.184450 | -0.058500 |
| 0.187943 | 0.065280 | 0.190643 | -0.059200 |
| 0.194133 | 0.066232 | 0.196915 | -0.059880 |
| 0.200399 | 0.067173 | 0.203264 | -0.060540 |
| 0.206777 | 0.068101 | 0.209650 | -0.061182 |
| 0.213232 | 0.069012 | 0.216106 | -0.061808 |
| 0.219758 | 0.069907 | 0.222633 | -0.062418 |
| 0.226356 | 0.070785 | 0.229229 | -0.063011 |
| 0.233023 | 0.071645 | 0.235893 | -0.063587 |
| 0.239758 | 0.072488 | 0.242622 | -0.064147 |
| 0.246559 | 0.073314 | 0.249416 | -0.064689 |
| 0.253424 | 0.074121 | 0.256272 | -0.065214 |
| 0.260352 | 0.074910 | 0.263190 | -0.065722 |
| 0.267340 | 0.075681 | 0.270166 | -0.066212 |
| 0.274388 | 0.076433 | 0.277200 | -0.066685 |
| 0.281493 | 0.077165 | 0.284290 | -0.067141 |
| 0.288654 | 0.077878 | 0.291434 | -0.067578 |
| 0.295869 | 0.078572 | 0.298630 | -0.067999 |
| 0.303136 | 0.079246 | 0.305876 | -0.068401 |
| 0.310453 | 0.079900 | 0.313171 | -0.068786 |
| 0.317818 | 0.080533 | 0.320513 | -0.069152 |
| 0.325230 | 0.081146 | 0.327900 | -0.069501 |
| 0.332687 | 0.081738 | 0.335331 | -0.069831 |
| 0.340187 | 0.082309 | 0.342803 | -0.070143 |
| 0.347728 | 0.082859 | 0.350315 | -0.070438 |
| 0.355309 | 0.083388 | 0.357864 | -0.070713 |
| 0.362926 | 0.083895 | 0.365450 | -0.070970 |

Upper SurfaceLower Surface

| x/c | y/c | x/c | y/c |
|----------|----------|----------|-----------|
| 0.370579 | 0.084381 | 0.373069 | -0.071209 |
| 0.378266 | 0.084845 | 0.380722 | -0.071430 |
| 0.385983 | 0.085287 | 0.388404 | -0.071632 |
| 0.393731 | 0.085706 | 0.396114 | -0.071815 |
| 0.401506 | 0.086104 | 0.403852 | -0.071981 |
| 0.409308 | 0.086479 | 0.411614 | -0.072127 |
| 0.417133 | 0.086831 | 0.419399 | -0.072255 |
| 0.424980 | 0.087161 | 0.427205 | -0.072364 |
| 0.432847 | 0.087469 | 0.435030 | -0.072455 |
| 0.440732 | 0.087753 | 0.442872 | -0.072527 |
| 0.448633 | 0.088014 | 0.450729 | -0.072580 |
| 0.456548 | 0.088252 | 0.458599 | -0.072614 |
| 0.464475 | 0.088467 | 0.466481 | -0.072631 |
| 0.472413 | 0.088660 | 0.474373 | -0.072628 |
| 0.480358 | 0.088828 | 0.482272 | -0.072607 |
| 0.488310 | 0.088974 | 0.490176 | -0.072567 |
| 0.496266 | 0.089096 | 0.498084 | -0.072508 |
| 0.504224 | 0.089194 | 0.505994 | -0.072430 |
| 0.512182 | 0.089271 | 0.513903 | -0.072335 |
| 0.520139 | 0.089324 | 0.521810 | -0.072222 |
| 0.528092 | 0.089356 | 0.529714 | -0.072092 |
| 0.536039 | 0.089365 | 0.537611 | -0.071944 |
| 0.543978 | 0.089351 | 0.545500 | -0.071779 |
| 0.551908 | 0.089315 | 0.553379 | -0.071596 |
| 0.559826 | 0.089257 | 0.561247 | -0.071396 |
| 0.567731 | 0.089177 | 0.569101 | -0.071178 |
| 0.575619 | 0.089074 | 0.576939 | -0.070943 |
| 0.583491 | 0.088949 | 0.584760 | -0.070691 |
| 0.591342 | 0.088801 | 0.592561 | -0.070422 |
| 0.599173 | 0.088632 | 0.600341 | -0.070136 |
| 0.606979 | 0.088441 | 0.608097 | -0.069832 |
| 0.614761 | 0.088228 | 0.615829 | -0.069511 |
| 0.622515 | 0.087992 | 0.623533 | -0.069174 |
| 0.630240 | 0.087735 | 0.631208 | -0.068819 |
| 0.637934 | 0.087456 | 0.638853 | -0.068447 |
| 0.645595 | 0.087155 | 0.646464 | -0.068059 |
| 0.653221 | 0.086834 | 0.654042 | -0.067654 |
| 0.660810 | 0.086490 | 0.661582 | -0.067232 |
| 0.668360 | 0.086125 | 0.669085 | -0.066794 |
| 0.675869 | 0.085739 | 0.676547 | -0.066339 |
| 0.683337 | 0.085332 | 0.683968 | -0.065867 |
| 0.690759 | 0.084903 | 0.691344 | -0.065380 |
| 0.698136 | 0.084455 | 0.698676 | -0.064875 |
| 0.705464 | 0.083985 | 0.705959 | -0.064355 |
| 0.712827 | 0.083492 | 0.713109 | -0.063822 |
| 0.720158 | 0.082968 | 0.720189 | -0.063284 |
| 0.727433 | 0.082414 | 0.727219 | -0.062738 |
| 0.734650 | 0.081830 | 0.734197 | -0.062187 |
| 0.741807 | 0.081216 | 0.741121 | -0.061629 |
| 0.748903 | 0.080574 | 0.747991 | -0.061065 |

Upper SurfaceLower Surface

| x/c | y/c | x/c | y/c |
|----------|----------|----------|-----------|
| 0.755936 | 0.079902 | 0.754803 | -0.060494 |
| 0.762904 | 0.079203 | 0.761556 | -0.059917 |
| 0.769805 | 0.078476 | 0.768250 | -0.059332 |
| 0.776638 | 0.077721 | 0.774881 | -0.058740 |
| 0.783400 | 0.076940 | 0.781449 | -0.058141 |
| 0.790091 | 0.076133 | 0.787953 | -0.057535 |
| 0.796708 | 0.075300 | 0.794390 | -0.056921 |
| 0.803249 | 0.074442 | 0.800759 | -0.056299 |
| 0.809715 | 0.073560 | 0.807058 | -0.055670 |
| 0.816101 | 0.072652 | 0.813287 | -0.055032 |
| 0.822407 | 0.071711 | 0.819442 | -0.054386 |
| 0.828631 | 0.070743 | 0.825524 | -0.053732 |
| 0.834771 | 0.069749 | 0.831530 | -0.053069 |
| 0.840828 | 0.068734 | 0.837459 | -0.052397 |
| 0.846797 | 0.067698 | 0.843309 | -0.051716 |
| 0.852679 | 0.066642 | 0.849080 | -0.051027 |
| 0.858472 | 0.065567 | 0.854769 | -0.050328 |
| 0.864173 | 0.064472 | 0.860376 | -0.049619 |
| 0.869783 | 0.063360 | 0.865899 | -0.048902 |
| 0.875299 | 0.062229 | 0.871336 | -0.048174 |
| 0.880720 | 0.061081 | 0.876686 | -0.047436 |
| 0.886045 | 0.059918 | 0.881948 | -0.046688 |
| 0.891272 | 0.058738 | 0.887121 | -0.045931 |
| 0.896401 | 0.057544 | 0.892203 | -0.045162 |
| 0.901430 | 0.056335 | 0.897193 | -0.044383 |
| 0.906357 | 0.055111 | 0.902090 | -0.043594 |
| 0.911181 | 0.053876 | 0.906892 | -0.042793 |
| 0.915903 | 0.052628 | 0.911598 | -0.041982 |
| 0.920519 | 0.051367 | 0.916207 | -0.041160 |
| 0.925030 | 0.050096 | 0.920719 | -0.040326 |
| 0.929434 | 0.048814 | 0.925131 | -0.039482 |
| 0.933729 | 0.047522 | 0.929443 | -0.038625 |
| 0.937916 | 0.046221 | 0.933653 | -0.037758 |
| 0.941993 | 0.044911 | 0.937761 | -0.036878 |
| 0.945960 | 0.043594 | 0.941765 | -0.035988 |
| 0.949813 | 0.042268 | 0.945665 | -0.035103 |
| 0.953555 | 0.040936 | 0.949317 | -0.034220 |
| 0.957183 | 0.039598 | 0.951587 | -0.033365 |
| 0.960696 | 0.038256 | 0.953807 | -0.033012 |
| 0.964094 | 0.036907 | 0.955977 | -0.032406 |
| 0.967377 | 0.035554 | 0.958098 | -0.031793 |
| 0.968765 | 0.034959 | 0.960168 | -0.031176 |
| 0.968765 | 0.034793 | 0.962188 | -0.030554 |
| 0.968352 | 0.032529 | 0.964156 | -0.029926 |
| 0.969284 | 0.032390 | 0.966075 | -0.029289 |
| 0.971078 | 0.032056 | 0.967942 | -0.028648 |
| 0.972819 | 0.031655 | 0.969757 | -0.027987 |
| 0.974507 | 0.031193 | 0.971522 | -0.027315 |
| 0.976142 | 0.030671 | 0.973235 | -0.026638 |
| 0.977722 | 0.030097 | 0.974896 | -0.025958 |

Upper SurfaceLower Surface

| x/c | y/c | x/c | y/c |
|----------|----------|----------|-----------|
| 0.979251 | 0.029495 | 0.976505 | -0.025261 |
| 0.980726 | 0.028878 | 0.978062 | -0.024551 |
| 0.982147 | 0.028213 | 0.979566 | -0.023845 |
| 0.983513 | 0.027518 | 0.981018 | -0.023124 |
| 0.984829 | 0.026800 | 0.982417 | -0.022407 |
| 0.986090 | 0.026063 | 0.983763 | -0.021675 |
| 0.987297 | 0.025294 | 0.985056 | -0.020950 |
| 0.988450 | 0.024503 | 0.986296 | -0.020224 |
| 0.989549 | 0.023698 | 0.987482 | -0.019484 |
| 0.990594 | 0.022883 | 0.988616 | -0.018729 |
| 0.991584 | 0.022047 | 0.989696 | -0.017926 |
| 0.992521 | 0.021189 | 0.990724 | -0.017105 |
| 0.993402 | 0.020290 | 0.991697 | -0.016254 |
| 0.994229 | 0.019334 | 0.992619 | -0.015351 |
| 0.994999 | 0.018327 | 0.993485 | -0.014429 |
| 0.995715 | 0.017290 | 0.994300 | -0.013457 |
| 0.996376 | 0.016248 | 0.995061 | -0.012447 |
| 0.996982 | 0.015186 | 0.995767 | -0.011429 |
| 0.997534 | 0.014093 | 0.996421 | -0.010370 |
| 0.998029 | 0.012956 | 0.997019 | -0.009304 |
| 0.998470 | 0.011815 | 0.997564 | -0.008197 |
| 0.998857 | 0.010659 | 0.998054 | -0.007081 |
| 0.999185 | 0.009464 | 0.998491 | -0.005941 |
| 0.999461 | 0.008247 | 0.998873 | -0.004775 |
| 0.999680 | 0.006975 | 0.999199 | -0.003614 |
| 0.999846 | 0.005778 | 0.999474 | -0.002392 |
| 0.999954 | 0.004463 | 0.999694 | -0.001158 |
| 1.000000 | 0.002799 | 0.999858 | 0.000065 |
| | | 0.999971 | 0.001476 |
| | | 1.000000 | 0.002799 |

Bibliography

1. Abramson, J. and E.O. Rogers. "High-Speed Characteristics of Circulation Control Airfoils," AIAA 21st Aerospace Sciences Meeting. Paper No 83-0265. New York: American Institute of Aeronautics and Astronautics, January 1983.
2. Baldwin, B.S. and H. Lomax. "Thin Layer Approximation and Algebraic Model for Separated Turbulent Flows," AIAA 16th Aerospace Sciences Meeting. Paper No 78-257. New York: American Institute of Aeronautics and Astronautics, January 1978.
3. Beam, Richard M. and R.F. Warming. "An Implicit Factored Scheme for the Compressible Navier-Stokes Equations," AIAA 3rd Computational Fluid Dynamics Conference. Paper No 77-645. New York: American Institute of Aeronautics and Astronautics, 1977.
4. Berman, H.A. "A Navier-Stokes Investigation of a Circulation Control Airfoil," AIAA 23rd Aerospace Sciences Meeting. Paper 85-0300. New York: American Institute of Aeronautics and Astronautics, January 1985.
5. Bradshaw, P. "Effects of Streamline Curvature on Turbulent Flow," AGARDograph No 169. London: Technical Editing and Reproduction Ltd, August 1973.
6. Dorrell, E.W., Jr. and B.K. Soni. INGRID: Interactive Two-Dimensional Grid Generation. AEDC-TR-86-49. Arnold Air Force Station, TN: AEDC/DOS, February 1987.
7. Dvorak, Frank A. and Do Hyung Choi. The Development of an Analytic Method for Two-Dimensional Circulation-Control Airfoils in Transonic Flow. Contract N00167-81-C-0041. Redmond WA: Analytical Methods, Inc., September 1981.
8. Kohlman, David L. Introduction to V/STOL Airplanes. Ames, IO: Iowa State University Press, 1981.
9. Nielsen, Jack N. and James C. Biggers. "Recent Progress in Circulation Control Aerodynamics," AIAA 25th Aerospace Sciences Meeting. Paper 87-0001. New York: American Institute of Aeronautics and Astronautics, January 1987.
10. Pulliam, Thomas H. et al. "Navier-Stokes Computations for Circulation Control Airfoils," Proceedings of the Circulation-Control Workshop 1986. NASA CP-2432:135-164. Washington: NASA, May 1987.
11. Schlichting, Hermann. Boundary-Layer Theory (Seventh Edition). New York: McGraw-Hill Book Company, 1979.

12. Shrewsbury, George D. "Analysis of Circulation Control Airfoils Using an Implicit Navier-Stokes Solver," AIAA 23rd Aerospace Sciences Meeting. Paper 85-0171. New York: American Institute of Aeronautics and Astronautics, January 1985.
13. ----- . "Evaluation of a Research Circulation Control Airfoil Using Navier-Stokes Methods," AIAA 25th Aerospace Sciences Meeting. Paper 87-0002. New York: American Institute of Aeronautics and Astronautics, January 1987.
14. ----- . "Numerical Evaluation of Circulation Control Airfoil Performance Using Navier-Stokes Methods," AIAA 24th Aerospace Sciences Meeting. Paper 86-0286. New York: American Institute of Aeronautics and Astronautics, January 1986.
15. Visbal, M.R. Calculation of Viscous Transonic Flows About a Supercritical Airfoil. AFWAL-TR-86-3013. Wright-Patterson Air Force Base, OH: AFWAL/FIMM, July 1986.
16. ----- . "Evaluation of an Implicit Navier-Stokes Solver for Some Unsteady Separated Flows," AIAA/ASME 4th Fluid Mechanics, Plasma Dynamics and Lasers Conference. Paper 86-1053. New York: American Institute of Aeronautics and Astronautics, May 1986.
17. ----- and J.S. Shang. "Numerical Investigation of the Flow Structure around a Rapidly Pitching Airfoil," AIAA 19th Fluid Dynamics, Plasma Dynamics and Lasers Conference. Paper 87-1424. New York: American Institute of Aeronautics and Astronautics, June 1987.
18. Wood, N. and J. Nielsen. "Circulation Control Airfoils Past, Present and Future," AIAA 23rd Aerospace Sciences Meeting. Paper 85-0204. New York: American Institute of Aeronautics and Astronautics, January 1985.

Vita

Steven L. Williams was born on 5 December 1961 in Two Harbors, Minnesota. He graduated in 1980 from Connersville High School in Connersville, Indiana and then attended Purdue University from which he received the degree of Bachelor of Science in Aeronautical and Astronautical Engineering in May 1984. Upon graduation, he began studies toward a masters degree at Purdue University before becoming employed as an aerodynamicist in the Engineering Directorate at Wright-Patterson AFB, Ohio. In January 1985, he entered the School of Engineering, Air Force Institute of Technology as a part-time student. In September 1988, he accepted a position in the Directorate of Development Planning at Wright-Patterson AFB, Ohio, as an aircraft preliminary design engineer specializing in the field of aerodynamics.

Permanent address: 4284 East Patterson Road
Beavercreek, Ohio 45430

REPORT DOCUMENTATION PAGE

Form Approved
OMB No. 0704-0188

| | | | |
|--|--|---|--------------------------------|
| 1a. REPORT SECURITY CLASSIFICATION UNCLASSIFIED | | 1b. RESTRICTIVE MARKINGS | |
| 2a. SECURITY CLASSIFICATION AUTHORITY | | 3. DISTRIBUTION / AVAILABILITY OF REPORT Approved for public release; distribution unlimited. | |
| 2b. DECLASSIFICATION / DOWNGRADING SCHEDULE | | 5. MONITORING ORGANIZATION REPORT NUMBER(S) | |
| 4. PERFORMING ORGANIZATION REPORT NUMBER(S) AFIT/GAE/AA/89M-4 | | 7a. NAME OF MONITORING ORGANIZATION | |
| 6a. NAME OF PERFORMING ORGANIZATION School of Engineering | 6b. OFFICE SYMBOL (if applicable) AFIT/ENG | 7b. ADDRESS (City, State, and ZIP Code) | |
| 6c. ADDRESS (City, State, and ZIP Code) Air Force Institute of Technology Wright-Patterson AFB, Ohio 45433-6583 | | 9. PROCUREMENT INSTRUMENT IDENTIFICATION NUMBER | |
| 8a. NAME OF FUNDING / SPONSORING ORGANIZATION USAF | 8b. OFFICE SYMBOL (if applicable) ASD/XRHI | 10. SOURCE OF FUNDING NUMBERS | |
| 8c. ADDRESS (City, State, and ZIP Code) WPAFB, OH 45433-6583 | | PROGRAM ELEMENT NO. | PROJECT NO. |
| | | TASK NO. | WORK UNIT ACCESSION NO. |
| 11. TITLE (Include Security Classification) USE OF NAVIER-STOKES METHODS TO PREDICT CIRCULATION CONTROL AIRFOIL PERFORMANCE | | | |
| 12. PERSONAL AUTHOR(S) Steven L. Williams, B.S. | | | |
| 13a. TYPE OF REPORT MS Thesis | 13b. TIME COVERED FROM _____ TO _____ | 14. DATE OF REPORT (Year, Month, Day) 1989 March | 15. PAGE COUNT 84 |
| 16. SUPPLEMENTARY NOTATION | | | |
| 17. COSATI CODES | | 18. SUBJECT TERMS (Continue on reverse if necessary and identify by block number) | |
| FIELD | GROUP | Aerodynamics; Boundary-Layer Control; Circulation Control; High Lift; Navier-Stokes Equations | |
| 20 | 04 | | |
| 19. ABSTRACT (Continue on reverse if necessary and identify by block number) | | | |
| Thesis Advisor: Milton E. Franke Professor Department of Aeronautics and Astronautics | | | |
| 20. DISTRIBUTION / AVAILABILITY OF ABSTRACT <input checked="" type="checkbox"/> UNCLASSIFIED/UNLIMITED <input type="checkbox"/> SAME AS RPT. <input type="checkbox"/> DYC USERS | | 21. ABSTRACT SECURITY CLASSIFICATION UNCLASSIFIED | |
| 22a. NAME OF RESPONSIBLE INDIVIDUAL Milton E. Franke, Professor | | 22b. TELEPHONE (Include Area Code) (513) 255-2362 | 22c. OFFICE SYMBOL AFIT/ENY |

The predictive capability of the two-dimensional compressible mass-averaged Navier-Stokes equations was investigated for a typical circulation control airfoil. The governing equations were solved using the implicit approximate factorization algorithm of Beam-Warming with the turbulence model of Baldwin-Lomax. To account for the unique characteristic of circulation control airfoils, an empirical turbulence model correction due to Bradshaw was employed. This study is unique in that the predictive capability of the computational method is explored by examining the importance of the empirical Bradshaw curvature correction constant on the computed results.

Using a generic value of the curvature constant at various blowing coefficient levels, the computational method was able to accurately predict the airfoil pitching moment and lift curve slope due to blowing. Predicted levels of airfoil lift coefficient, although reasonable, were found to be consistently low compared with experiment due to the generic curvature constant providing premature jet detachment from the Coanda surface. Computed and measured airfoil drag results followed the same trends, but the lack of overall drag coefficient agreement was somewhat disappointing.

Lift coefficient was found to be quite sensitive, pitching moment not sensitive, and drag coefficient moderately sensitive to the value of curvature constant used. For the highest blowing coefficient case considered, the value of curvature constant required for the computational lift coefficient to match the experimental lift coefficient was also determined. Using the experimentally correlated curvature constant, very good agreement between the computational and experimental pressure distributions was found. *Key point: Boundary layer separation, etc.*

In spite of the sensitivity of the computational results to the Bradshaw curvature correction constant, the method provided relatively accurate predictions of airfoil performance for the circulation control airfoil used in this study. Based on this result, the computational method shows promise as a circulation control airfoil design tool.